Computers in Biology and Medicine 102 (2018) 57–74

Contents lists available at ScienceDirect

Computers in Biology and Medicine

journal homepage: www.elsevier.com/locate/compbiomed

Generalized polynomial chaos-based uncertainty quantification and propagation in multi-scale modeling of cardiac electrophysiology

Zhiyong Hu[a], Dongping Du[a,*], Yuncheng Du[b,**]

[a] Department of Industrial, Manufacturing and Systems Engineering, Texas Tech University, Lubbock, TX, 79409, USA
[b] Department of Chemical and Biomolecular Engineering, Clarkson University, Potsdam, NY, 33613, USA

ARTICLE INFO

Keywords:
Uncertainty propagation
Cardiac electrophysiology
Sensitivity analysis
Stochastic model
Mouse ventricular myocyte

ABSTRACT

Uncertainty and physiological variability are ubiquitous in cardiac electrical signaling. It is important to address the uncertainty and variability in cardiac modeling to provide reliable and realistic predictions of heart function, thus ensuring trustworthy computer-aided medical decision-making and treatment planning. Statistical techniques such as Monte Carlo (MC) simulations have been applied to uncertainty quantification and propagation in cardiac modeling. However, MC simulation-based methods are computationally prohibitive for complex cardiac models with a great number of parameters and governing equations. In this paper, we propose to use the Generalized Polynomial Chaos (gPC) expansion in combination with Galerkin projection to analytically quantify parametric uncertainty in ion channel models of mouse ventricular cell, and further propagate the uncertainty across different organizational levels of cell and tissue. To identify the most significant parametric uncertainty in cardiac ion channel and cell models, variance decomposition-based sensitivity analysis was first performed. Following this, gPC was integrated with deterministic cardiac models to propagate uncertainty through ion current, ventricular cell, 1D cable, and 2D tissue to account for the stochasticity and cell-to-cell variability. As compared to MC, the gPC in this work shows the superior performance in terms of computational efficiency. In addition, the gPC models can provide a measure of confidence in model predictions, which can improve the reliability of computer simulations of cardiac electrophysiology for clinical applications.

1. Introduction

Mathematical models of cardiac electrophysiology have been widely used to advance the fundamental understanding of etiology and pathophysiology of cardiac diseases, aid clinical diagnosis and prognosis, and assist therapeutic design and treatment development. Since Noble's first attempt to study the electrophysiology of a single cell with the Hodgkin-Huxley model [1,2], cardiac models have become more detailed due to the increased knowledge of ion channel gating and cardiac electrical signaling. Current models of cardiac electrophysiology are multiscale and highly complex, which integrate models across different organizational levels of ion channel, cell, tissue, and the organ [3]. These models have been used to examine cardiac disease mechanisms, optimize treatment and surgical planning. For example, the whole-heart model has been applied in clinical settings to localize ablation therapy [4], terminate cardiac arrhythmias [5], and design cardiac resynchronization therapy [6].

While cardiac models have shown the potentials, applications such as model-based diagnosis and therapeutic design are still limited due to the incapability of accounting for uncertainty and variability among individuals [7]. Uncertainty may originate from model assumptions, calibration of model parameters using noisy data, intrinsic time varying phenomena, and extrinsic cell-to-cell variability [8,9]. For example, physiological variability constantly presents in ion channel gating, cardiac electrical signaling, and electrical propagation in cardiac tissue, due to the stochastic nature of ion channel gating [10] and the nonlinear dynamics of alternans in cardiac action potential duration (APD) [8]. In addition, Action Potential (AP) may change from cell to cell due to quantities that genuinely vary among cells, e.g., cell size and ion channel expression [11]. However, most of the available cardiac models are deterministic with fixed model parameters, which cannot account for uncertainty. If the uncertainty in the cardiac models is not appropriately addressed, computer experiments may fail to provide reliable predictions and lead to false conclusions, thus misleading medical decisions [7].

* Corresponding author.
** Corresponding author.
E-mail addresses: dongping.du@ttu.edu (D. Du), ydu@clarkson.edu (Y. Du).

https://doi.org/10.1016/j.compbiomed.2018.09.006
Received 13 February 2018; Received in revised form 11 September 2018; Accepted 11 September 2018

To improve the credibility and reliability of cardiac models, it is necessary to quantify and propagate the uncertainty to obtain confident model predictions (outputs). Uncertainty quantification and propagation techniques have been well developed in engineering and science domains [12]. Computer models are often developed and calibrated with data corrupted by various sources of uncertainty, which in turn may introduce uncertainty in model parameters. Uncertainty quantification and propagation typically assign probability distributions to model parameters to represent parametric uncertainty, which can subsequently be propagated onto model outputs to obtain a measure of confidence in model predictions. Uncertainty quantification in cardiac models has been previously studied [7,11–14]. For example, Romero et al. investigated the effect of variability in ionic current on AP in human ventricular myocytes [15]. Pathmanathan et al. [7] quantified the variability in the steady-state inactivation of fast sodium current among *canine epi* and *endocardial* cells, and further propagated the uncertainty onto higher organizational levels to study the stochasticity in upstroke velocity in AP and spiral wave dynamics in 2D tissue. Although different uncertainty quantification methods were reported, efficient algorithms that can be used to propagate parametric uncertainty onto higher organizational scales in cardiac models have not been extensively investigated [7,16].

Sampling-based techniques such as Monte Carlo (MC) simulations are one of the most popular methods to propagate parametric uncertainty onto model outputs [17]. For MC, samples are randomly generated from the distribution of model parameters, simulations are then performed with each sample. Based on the simulation results, the variability in model outputs is approximated from a collection of the simulated outputs. It should be noted that MC may require a large number of simulations to ensure the convergence of the model predictions [18], which can be computationally prohibitive for complex and nonlinear cardiac models. To reduce the computational burden and improve the accuracy of uncertainty propagation, this work presents a non-sampling based uncertainty analysis technique, i.e., generalized polynomial chaos (gPC) expansion [19]. The gPC generally approximates the distribution of parametric uncertainty with orthogonal polynomial basis functions and propagates the uncertainty onto model predictions (outputs) through first-principles models. One advantage of the gPC is that it can provide analytical expressions of the statistical moments of model predictions. As compared to MC, uncertainty propagation with gPC has been proved to be more efficient in terms of computational time in different modeling, control, and optimization problems [18,20–24]. Geneser et al. [16] introduced uncertainty in rate coefficients of ion channel model, and applied gPC for uncertainty propagation in ion channel gating. However, uncertainty was randomly assigned to model parameters and the quantification of uncertainty was only studied at the ion channel level, which cannot provide the information about the effect of uncertainty on higher organizational levels such as cell and tissue. Using gPC, our previous work successfully propagated parametric uncertainty onto K^+ channel models [25]. However, the uncertainty propagation in higher organizational levels was not studied.

Uncertainty propagation in cardiac models is challenging, since models of cardiac electrophysiology are inherently multiscale and involve a great level of complexity. These models generally integrate cellular activities with tissue functions, where cellular activities are regulated by the orchestrated function of transmembrane currents and tissue functions are modeled as spatial-temporal propagation of electrical waves. The cellular models often include numerous differential equations coupled with over a hundred supporting equations. Further, the cellular models can serve as sub-models of the tissue models, which describe the electrical propagation in 2D/3D cardiac muscles using partial differential equations (PDEs) and finite elements meshes. The complexity of cardiac models poses great challenges on the gPC-based uncertainty propagation as the coupled differential equations and supporting equations can make it difficult to quantify uncertainty in model outputs resulting from parametric uncertainty. The objective in this work is to: (*i*) investigate the feasibility of the gPC-based uncertainty propagation in multiscale cardiac models across different organizational levels of ion channel, cell, and tissue, and (*ii*) quantify the effect of parametric uncertainty on model predictions in each organizational level in a computationally efficient manner.

Cardiac models are described by many equations involving hundreds of parameters. It is possible but not practical to consider uncertainty in all model parameters. To improve efficiency, we propose to identify the most sensitive parametric uncertainty. To identify the most significant uncertainty, sensitivity analysis techniques can be used. For example, Du et al. [3] used fractional factorial design to find sensitive parameters under different response functions for model calibration, and Johnstone et al. [8] used Gaussian process to find parametric uncertainty in cardiac models. However, these techniques concentrate on the sensitivity in the vicinity of the mean value of parameter and may fail to identify the most significant uncertainty. To overcome this issue, the variance decomposition-based sensitivity analysis method is used in this work to identify the parametric uncertainty that has the most significant impact on the variability in the outputs of ion channel models and the cardiac cell model. Based on the sensitivity analysis results, *a prior* known distribution will be assigned to the significant parameters to approximate uncertainty, which will be further propagated onto ion currents, cardiac cell, and tissue. Specifically, different characteristics, e.g., Steady State Activation (SSA) and Inactivation (SSI) in ion channel, APDs in cardiac cell, and spiral wave propagation in tissue, are quantified in order to visualize the effect of parametric uncertainty on model outputs. Additionally, the efficiency and accuracy of gPC are investigated and verified with MC simulations. Note that for algorithm clarification the Bondarenko's mouse ventricular model [26] is used in this work for propagating parametric uncertainty onto higher organizational levels of heart through multiscale cardiac models. We deliberately chose this model since it can provide detailed gating kinetics in ion channels, and it is considered sufficiently complicated to illustrate the computational efficiency of gPC.

The rest of this paper is organized as follows. Section 2 presents the research methodologies followed by design of computer experiments in Section 3. Simulation results and discussion are provided in Sections 4 and 5, which is followed by conclusions in Section 6.

2. Background and methodologies

2.1. Generalized polynomial chaos expansion

The generalized polynomial chaos (gPC) expansion approximates uncertainty as a function of another random variable based on a prescribed distribution from Askey-Wiener scheme [19]. Suppose a cardiac model can be defined with a nonlinear ordinary differential equation (ODE) as:

$$\frac{dy}{dt} = g(t, \sigma, \theta, y), \qquad 0 \le t \le T, \quad y(0) = y_0 \tag{1}$$

where g is a nonlinear function of cardiac model, e.g., the ion channel model, and y is a gating variable (i.e., output), e.g., the gating variable of activation or inactivation, with initial condition y_0 over a finite time domain $[0, T]$, θ and σ are model parameters. In this current work, θ denotes a vector of parametric uncertainties (i.e. input uncertainty) while σ is a vector of deterministic parameters defined with fixed values. Note that each parametric uncertainty in θ will be described with a probability density function (PDF) around a particular mean value and specific variance in this work. The uncertainty in each parameter of θ may originate from time-varying phenomena such as stochasticity in

channel gating or may result from extrinsic cell-to-cell variability. It should be noted that, when experimental data are available, the PDF of each parameter can be calibrated with experimental data using offline parameter estimation techniques such as the least squares fitting. Otherwise, the PDF can be inferred from other information such as empirical knowledge. In this work, the PDF of each parameter is assumed to be known, and the statistical distribution of each parameter in θ is time-invariant for simplicity.

Using the gPC expansion, the first step is to re-write each parameter θ_i in θ as a function of a random variable ξ_i as:

$$\theta_i(\xi_i) = \sum_{k=0}^{\infty} \hat{\theta}_{i,k}\Phi_k(\xi_i) \approx \sum_{k=0}^{q} \hat{\theta}_{i,k}\Phi_k(\xi_i)\,, \qquad i = 1,\ \cdots, n_\theta\,, \tag{2}$$

where $\Phi_k(\xi_i)$ is the orthogonal polynomial chaos basis function of parameter θ_i [19], $\hat{\theta}_{i,k}$ is the gPC coefficients of the ith parameter θ_i, which can be calculated through parameter estimation techniques, e.g., Maximum Likelihood Estimation, such that Eq. (2) follows *a prior* known PDF of θ_i, n_θ is the total number of parameters in θ. The random variables that can be used to approximate the parametric uncertainty of θ, i.e., $\xi = \{\xi_i\}$, are assumed to be independent in this work.

Since model parameters can affect model predictions (outputs) through the cardiac model g in Eq. (1), it is necessary to estimate their effect on the model outputs. Similar to the gPC expansion of parameters θ, the model prediction can be estimated in terms of the random vector $\xi = \{\xi_i\}$ as follows:

$$y = \hat{y}_0\Psi_0 + \sum_{i=1}^{n_\theta} \hat{y}_i\Psi_1(\xi_i) + \sum_{i=1}^{n_\theta}\sum_{j=1}^{i} \hat{y}_{i,j}\Psi_2(\xi_i, \xi_j) + \ldots \tag{3}$$

where $\hat{y}_i$ and $\hat{y}_{i,j}$ are the gPC coefficients that estimate the PDF profile of the model prediction y, which describes the uncertainty in model output resulting from parametric uncertainty θ, $\Psi_k(\xi)$ $k = 0, 1, 2 \ldots$ is the multivariate orthogonal polynomial basis function of random vector ξ defined as the product of univariate basis functions Φ_k's [18]. For simplicity, Eq. (3) can be rewritten as:

$$y = \sum_{k=0}^{\infty} \hat{y}_k\Psi_k(\xi) \approx \sum_{k=0}^{Q} \hat{y}_k\Psi_k(\xi)\,, \tag{4}$$

It should be noted that infinite terms are needed in Eq. (2) and Eq. (4) in order to approximate an arbitrary random variable with the gPC expansions. However, for practical application purposes, the expansion will be truncated into a finite number of terms. In this work, we used the *total-order expansion scheme* [27] to determine the number of terms in Eq. (4). The detailed explanation of how the *total-order expansion* operates is given in Appendix A, and the empirical formula that can be used to determine the necessary terms in both approximations is given as below.

The total number of terms Q in Eq. (4), according to the gPC approximation, can be determined as [28]:

$$Q = \left(\frac{(n_\theta + q)!}{n_\theta! q!}\right) - 1, \tag{5}$$

As seen in Eq. (5), the number of terms used in model predictions increases as the polynomial order q and/or the number of parametric uncertainties n_θ increases. Different from the calculation of gPC coefficients of parametric uncertainty θ, the gPC coefficients $\{\hat{y}_k\}$ of the model outputs can be calculated from the cardiac model g in combination with the Galerkin projection, which will be described as follows.

Using Galerkin projection, it is possible to determine the gPC coefficients $\{\hat{y}_k\}$ of model predictions by substituting Eq. (2) and Eq. (4) into Eq. (1), and by projecting Eq. (1) onto each one of the polynomial chaos basis functions $\{\Psi_k(\xi)\}$ as:

$$< \sum_{k=0}^{Q} \frac{d\hat{y}_k}{dt}\Psi_k(\xi), \Psi_j(\xi) > \ = \ < g\left(t, \sigma, \hat{\theta}, \sum_{k=0}^{Q} \hat{y}_k\Psi_k(\xi)\right), \Psi_j(\xi) > , \qquad j = 0, \ldots, Q \tag{6}$$

where $\hat{\theta}$ represents the gPC coefficient of θ, $\langle\cdot\rangle$ is an inner product between two functions, which is calculated as:

$$\int_{\Omega} \Psi(\xi) * \Psi'(\xi) * W(\xi)\, d\xi\ , \tag{7}$$

where Ω is the entire domain of the random variables ξ used to approximate parametric uncertainty θ, and $W(\xi)$ is the weighting function, i.e. probability density function (PDF) of ξ. The integral in Eq. (7) can be solved numerically with sparse quadrature rule [18]. In addition, it is important to note that the polynomial basis functions here are chosen *per* the option of the distribution of ξ to ensure orthogonality [18]. For example, Legendre polynomials are the choice of uniformly distributed random variables, while Hermite polynomials can be chosen for normally distributed random variables. Using the Galerkin projection and given the orthogonal property of the polynomials, the original cardiac model, i.e., Eq. (1), can be transformed into a set of coupled deterministic equations with unknown gPC coefficients (i.e., $\hat{y}_k$) of model predictions as:

$$\frac{d\hat{y}_j}{dt} = \frac{<g(t, \sigma, \hat{\theta}, \sum_{k=0}^{Q} \hat{y}_k\Psi_k(\xi)),\ \Psi_j(\xi)>}{<\Psi_j(\xi), \Psi_j(\xi)>} \qquad j = 0, \ldots, Q\ , \tag{8}$$

As seen, the only unknown in the coupled equations system is the gPC expansion coefficients, which can be solved with numerical methods such as Runge-Kutta [29]. Once these gPC coefficients are obtained, model predictions can be approximated by substituting these gPC coefficients into Eq. (4) at each time interval. In addition, the statistical moments of the model prediction y can be analytically approximated as follows.

$$\mathbb{E}(y) = \mathbb{E}\left[\sum_{k=0}^{Q} \hat{y}_k\Psi_k\right] = y_0\mathbb{E}[\Psi_0] = y_0\,, \tag{9}$$

$$\mathbb{V}(y) = \mathbb{E}\left[\left(\sum_{k=0}^{Q} \hat{y}_k\Psi_k - y_0\right)^2\right] = \mathbb{E}\left[\left(\sum_{k=1}^{Q} \hat{y}_k\Psi_k\right)^2\right] = \sum_{k=1}^{Q} \hat{y}_k^2\,, \tag{10}$$

The key of using gPC in this work is that it can analytically infer the stochasticity in model predictions (outputs) with Eqs. (9) and (10). This can significantly reduce the computation time required by uncertainty quantification, as the gPC coefficients can be easily solved which saves a large number of simulations as compared with MC methods. The discussion of the computation time will be given in the results section. In addition to the fast calculation of these statistical moments of model outputs, the distribution of the model predictions can be quantified by sampling ξ from *a prior* distribution and by substituting these samples into the gPC approximation of model outputs y in Eq. (4), which can be performed in a real-time fashion. The rapid calculation of uncertainty in model outputs, resulting from parametric uncertainty, is the main rationale for using the gPC approximation in this work, since this can necessitate efficient uncertainty propagation as compared to MC simulations. To better demonstrate the procedures of uncertainty propagation with gPC, an example using the activation gate variable of cardiac models is given in Appendix B.

2.2. Multiscale models of cardiac electrophysiology

Cardiac models of various species have been developed previously, which can provide sufficient details for describing cardiac functions across multiple organizational levels of ion channel, cell, tissue, and the

Table 1
Detailed expression of parameters in K^+ ion currents.

Transient outward K^+ current

$I_{Kto}I_{Kto} = G_{to}a_{to}^3 i_{to}(V - E_K)$

$\frac{da_{to}}{dt} = \alpha_a(1 - a_{to}) - \beta_a a_{to}$ $\frac{di_{to}}{dt} = \alpha_i(1 - i_{to}) - \beta_i i_{to}\alpha_a$ =

$p_1\exp(p_2(V + p_3))\beta_a$ = $p_4\exp(p_5(V + p_3))\alpha_i$ =

$p_6\exp(-(V + p_7)/p_8)/(p_9\exp(-(V + p_{10})/p_8) + 1)\beta_i$ =

$p_{11}\exp((V + p_{10})/p_8)/(p_{12}\exp((V + p_{10})/p_8) + 1)$

Delayed rectifier K^+ current

$I_{Kur}I_{Kur} = G_{ur}a_{ur}i_{ur}(V - E_K)\frac{da_{ur}}{dt} = \frac{a_{ss} - a_{ur}}{\tau_{aur}}$ $\frac{di_{ur}}{dt} = \frac{i_{ss} - i_{ur}}{\tau_{iur}}$

$a_{ss} = 1/\left(1 + \exp\left(-\frac{V+p_{13}}{p_{14}}\right)\right)$ $i_{ss} = 1/\left(1 + \exp\left(-\frac{V+p_{15}}{p_{16}}\right)\right)$

$\tau_{aur} = p_{17}\exp(p_{18}V) + p_{19}$ $\tau_{iur} = p_{20} - p_{21}/(1 + \exp((V + p_{15})/p_{16}))$

whole organ [3]. The ion channel gating is often described with either the Hodgkin Huxley type model or the Markov model, where gating kinetics are determined by activation and inactivation variables through ordinary differential equations (ODEs). For cardiac cells, the change of transmembrane potential over time is modeled as a function of ion currents, typically referred as Action Potential (AP). The electrophysiology of cardiac tissue is modeled with a reaction diffusion equation on mesh grids with each node defined as a cardiac cell. A collection of cell models, coupled through either monodomain or bidomain models, forms a spatial-temporal model to describe the electrical wave propagation in two/three-dimensional (2D/3D) tissue. In this current work, we will demonstrate the efficiency of the gPC-based uncertainty propagation using the Hodgkin-Huxley type K^+ channel models of the transient outward K^+ current (I_{Kto}), and the delayed rectifier K^+ current (I_{Kur}), mouse ventricular cell model [26], and monodomain tissue model [30]. It should be noted that K^+ currents are chosen, since they play important roles in the repolarization of AP and any slight changes in the currents can significantly affect the cardiac functions, thus leading to ventricular arrhythmias and life threatening cardiac events [31,32]. In addition, mouse ventricular cell model is used for algorithm clarification in this work, since mouse ventricular myocytes are widely used *in-vitro* experiments for investigating unknown etiology [33] and for testing drug efficiency [34]. We deliberately chose this model because it can provide detailed gating kinetics in ion channels, and it is considered sufficiently complicated to illustrate the computational efficiency of gPC.

2.2.1. Models of ion currents

For algorithm clarification, we first investigated the parametric uncertainty in ion channel models. Such parametric uncertainty may either result from the stochastic nature of ion channel gating or originate from cell-to-cell variability. Using gPC as explained in Section 2.1, the uncertainty is propagated onto two K^+ ion currents, i.e., I_{Kto} and I_{Kur}, which can be described by Hodgkin-Huxley type model as follows [26]:

$$I_{Kto} = G_{to}a_{to}^3 i_{to}(V - E_K)\ , \tag{11}$$

$$I_{Kur} = G_{ur}a_{ur}i_{ur}(V - E_K)\ , \tag{12}$$

where G_{to} and G_{ur} are conductance, a_{to} and a_{ur} are activation gating variables, i_{to} and i_{ur} are inactivation gating variables, E_K is the reverse potential (-82.8 mV), and V is the transmembrane potential. The equations of activation and inactivation variables are shown in Table 1, and the model parameters used in this work are given in Table 2 [26].

2.2.2. Model of mouse ventricular myocyte

The movement of ions such as K^+, Na^+, and Ca^{2+}, i.e., across cell membrane through ion channels, can lead to changes in membrane potential. Uncertainties in ion channel gating will jointly affect cellular activities, thus leading to variations in the AP in cardiac cells. In this work, mouse ventricular myocyte model developed by Bondarenko et al.'s [26] is used to study the effect of parametric uncertainty in ion channel on electrical signaling of cardiac cell. In Bondarenko et al.'s model, cell membrane is modeled as electrical circuit with subcellular compartmental space. Assuming there are no electrical gradients within the cell itself, the membrane potential is described as follows:

$$-C_m\frac{dV}{dt} = I_{CaL} + I_{p(Ca)} + I_{NaCa} + I_{Cab} + I_{Na} + I_{Nab} + I_{NaK} + I_{Kto} + I_{K1} + I_{Ks} + I_{Kur} + I_{Kss} + I_{Kr} + I_{Cl,Ca} + I_{stim}\ , \tag{13}$$

where t is time, C_m is the cell capacitance *per* unit surface area, I_{stim} is the external stimulus current, which activates the cell from the resting state. As seen in Eq. (13), the transmembrane currents incorporate L-type Ca^{2+} current I_{CaL}, sarcolemmal Ca^{2+} pump current $I_{\mathrm{p(Ca)}}$, Na^+/Ca^{2+} exchange current I_{NaCa}, background Ca^{2+} and Na^+ currents I_{Cab} and I_{Nab}, fast Na^+ current I_{Na}, rapidly recovering transient outward K^+ current I_{Kto}, rapid delayed rectifier K^+ current I_{Kr}, ultra-rapidly activating delayed rectifier K^+ current I_{Kur}, non-inactivating steady-state voltage-activated K^+ current I_{Kss}, time-independent inwardly rectifying K^+ current I_{K1}, slow delayed rectifier K^+ current I_{Ks}, Ca^{2+}-activated Cl^- current $I_{\mathrm{Cl,Ca}}$, and Na^+/K^+ pump current I_{NaK}. Modeling of ionic currents is based on either Hodgkin-Huxley or Markov-based formulations. For brevity, the details of each current kinetics and parameters used in this work are not given, but they can be found in Ref. [26]. The parametric uncertainty in K^+ currents of I_{Kto} and I_{Kur} were investigated in this work, since they are two major voltage-gated currents that are responsible for repolarization [32,35,36]. Note that the proposed uncertainty quantification technique can be easily extended to other currents with minor modifications.

2.2.3. Model of 1D cable and 2D tissue

Cardiac tissue is often modeled as a collection of cardiac cells connected with gap junctions. Each depolarized cell can stimulate its neighbor cells and trigger electrical conduction among tissue. We propose to study the *cell-to-cell* variability by propagating the uncertainties among cells into electrical activities at the tissue level. The electrical propagation on the one-dimensional (1D) cell string and the two-dimensional (2D) tissue was studied. The conduction of AP in the cell string and tissue was modeled using the following reaction diffusion equation:

$$\frac{\partial V}{\partial t} = -\frac{1}{C_m}\left(I_{ion} + I_{stim} + \frac{1}{\rho S}\nabla^2 V\right)\ , \tag{14}$$

Table 2
Parameter declaration of K^+ ion currents models.

I_{Kto}						I_{Kur}				
p_1	p_2	p_3	p_4	p_5	p_6	p_{13}	p_{14}	p_{15}	p_{16}	p_{17}
0.18,064	0.03577	30.0	0.395	−0.06237	0.000152	22.5	7.7	45.2	5.7	0.493
p_7	p_8	p_9	p_{10}	p_{11}	p_{12}	p_{18}	p_{19}	p_{20}	p_{21}	
13.5	7.0	0.067,083	33.5	0.00095	0.051,335	−0.0629	2.058	1200	170	

where C_m is the cell capacitance *per* unit surface area, I_{ion} is the sum of transmembrane ion currents, ρ is the cellular resistivity, S is the surface-to-volume ratio, and ∇^2 is the Laplacian operator, i.e., $\frac{\partial^2 V}{\partial x^2}$ for linear cable, and $\frac{\partial^2 V}{\partial x^2} + \frac{\partial^2 V}{\partial y^2}$ for 2D tissue, x and y determine the spatial coordinates of cells, respectively. To simulate the propagation of electric waves along 1D cell string, Eq. (14) is solved numerically with finite-difference scheme as:

$$V_{i,j}^{t+dt} - V_{i,j}^{t} = -\frac{dt}{C_m}\left\{(I_{ion} + I_{stim}) + \frac{1}{\rho S(dx)^2}(V_{i-1}^{t} + V_{i+1}^{t} - 2V_i^{t})\right\}\Bigg\} \tag{15}$$

Note that Neumann boundary condition was used in the 1D cable simulation. The numerical discretization scheme for the 2D tissue can be described as follows:

$$V_{i,j}^{t+dt} - V_{i,j}^{t} = -\frac{dt}{C_m}\left\{(I_{ion} + I_{stim}) + \frac{1}{\rho S(dx)^2}(V_{i-1,j}^{t} + V_{i+1,j}^{t} + V_{i-1,j}^{t} + V_{i,j-1}^{t} - 4V_{i,j}^{t})\right\}, \tag{16}$$

where no flux boundary condition is assumed to ensure that there are no current leakages on the boundaries.

2.3. Sensitivity analysis

Cardiac models often involve a great number of model parameters. For example, the model of I_{Kto} presented in the previous section involves 12 parameters. In addition, uncertainty in model parameters may have different effect on model predictions. The identification of the most sensitive parametric uncertainty is essential for efficient uncertainty propagation. A variance-based global sensitivity analysis algorithm in this work is developed to quantify the effect of parametric uncertainty on the variability of model predictions.

The variance-based sensitivity analysis can decompose the model outputs with respect to a set of samples of parametric uncertainty θ. A sensitivity index, i.e., Sobol Sensitivity Index (SI), can be used to quantify the fractional effect of parametric uncertainty on the variability of model outputs [37]. The SI not only provides a measure of the main effect of a particular parameter on the model predictions, but also evaluates the joint effect of interactions among parameters on the model outputs. Let us define the ion channel model described in Eq. (1) as $y = f(\boldsymbol{p})$ for simplicity, where $\boldsymbol{p} = \{p_i\}, i = 1, 2, \ldots n$, n is the number of model parameters in total. The model output $y = f(\boldsymbol{p})$ can be decomposed with respect to each parameter as [38]:

$$f(\boldsymbol{p}) = f_0 + \sum_{i=1}^{n} f_i(p_i) + \sum_{i=1}^{n}\sum_{j=i}^{n} f_{i,j}(p_i, p_j) + \ldots + f_{1,\ldots,n}(p_1, \ldots, p_n), \tag{17}$$

where f_0 is a constant that can be calculated as: $f_0 = \mathbb{E}(y)$, $f_i = \mathbb{E}(y|p_i) - \mathbb{E}(y)$, $f_{i,j} = \mathbb{E}(y|p_i, p_j) - f_i - f_j - \mathbb{E}(y)$.

The total variance can be calculated as:

$$\mathbb{V} = \int_{\Omega^n} f^2(\boldsymbol{p})d\boldsymbol{p} - f_0^2. \tag{18}$$

Further, the total variance can be decomposed in the similar manner as done in Eq. (17), which gives the following:

$$\mathbb{V} = \sum_{i=1}^{n} \mathbb{V}_i(p_i) + \sum_{i=1}^{n}\sum_{j=i}^{n} \mathbb{V}_{i,j}(p_i, p_j) + \ldots + \mathbb{V}_{1,\ldots,n}(p_1, \ldots, p_n), \tag{19}$$

where $\mathbb{V}_i = \mathbb{V}(\mathbb{E}(y|p_i))$, $\mathbb{V}_{i,j} = \mathbb{V}(\mathbb{E}(y|p_i, p_j)) - \mathbb{V}(\mathbb{E}(y|p_i)) - \mathbb{V}(\mathbb{E}(y|p_j)) - \mathbb{E}(y)$. We can further divide the variance associated with each parameter by the total unconditional variance of model predictions in order to calculate the SI as:

$$S_i = \frac{\mathbb{V}_i}{\mathbb{V}}, \tag{20}$$

which provides the main effect S_i of the i^{th} parameter p_i on the model output. Similarly, the second order SI can be estimated as:

$$S_{i,j} = \frac{\mathbb{V}_{i,j}}{\mathbb{V}}, \tag{21}$$

And the total effect of p_i on the model output can be calculated as:

$$S_{T_i} = S_i + \sum_{j=1}^{n} S_{i,j} + \sum_{j=1}^{n}\sum_{k=1}^{n} S_{i,j,k} + \ldots. \tag{22}$$

The main and total effects provide a measure of the significance of parametric uncertainty on model outputs. In this work, the SI of the main S_i and total effect S_{T_i} of each parameter are used to identify the most significant parametric uncertainties. Based on the sensitivity analysis results, the gPC approximation explained in Section 2.1 is used to approximate significant parametric uncertainty, which is then propagated onto different organizational levels such as cell and tissue in order to evaluate the effect of uncertainty on model predictions.

3. Design of experiments

3.1. Simulation protocols

The effects of parametric uncertainty on Steady State Activation (SSA), Steady State Inactivation (SSI), and current density (i.e., I–V relationship) are first investigated at the ion channel scale. To generate the model outputs of SSA, SSI, and I–V, we performed computer simulations using the K^+ current models of I_{Kto}, and I_{Kur}. The simulations follow standard experimental protocols, which are briefly described as follows.

Steady State Activation (SSA): Cell membrane potential (V) is first held at −100 mV for 200 ms, then steps to testing potentials varying from −50 mV to +50 mV with a 10 mV increment for 500 ms, followed by a step change to −100 mV. For each K^+ current, the model is solved accordingly to generate traces of ion current. The maximum steady state conductance can be determined as $G = I_{max}/(V - E_K)$, where I_{max} is the peak current at each testing potential V, and E_K is the reverse potential of the K^+ channel. The SSA is obtained by normalizing the maximum steady state conductance at each testing potential to the theoretical maximum conductance G_{max}. In addition, the peak current at each testing potential is recorded to generate current density (I–V relationship).

Steady State Inactivation (SSI): Simulations are performed for each K^+ current using the models described in Section 2.1, where cell membrane potential (V) is initially held at −70 mV before stepping to testing potentials (varying from −110 mV to 0 mV with a 10 mV increment) for 10 s, then steps to 30 mV for another 4.5 s before returning to −70 mV. The simulation can generate one trace of ion current at each testing potential, and the peak currents for these testing potentials are normalized with respect to the maximum peak current.

3.2. Sensitivity analysis

3.2.1. Ion currents

Variance-based sensitivity analysis is first performed to identify significant parametric uncertainties in K^+ currents, i.e., I_{Kto}, and I_{Kur}. Based on the sensitivity analysis results, a probability density function is assigned to each of these significant parameters in order to describe the uncertainty. The mathematical description of a significant parameter can be defined as:

$$\theta_i = \overline{\theta_i} + \Delta\theta_i\xi_i, \quad (i = 1, \ldots, n), \tag{23}$$

where n is the total number of significant parameters identified from the sensitivity analysis, θ_i is the *ith* parametric uncertainty, $\overline{\theta_i}$ denotes the mean value of the parametric uncertainty while $\Delta\theta_i$ is the parameter that can be used to define the stochastic variation (uncertainty) around

each mean value. In this work, each significant parameter is assumed to be normally distributed with a mean value equals to the nominal value given in Table 2, while two different variations ($\Delta\theta_i$) are used. That is, a standard deviation equals to a 5% of the mean value and a standard deviation equals to a 10% of the mean value. Again, it should be noted that, when actual measurements are available, the probability distribution of parameters can be calibrated with offline estimation techniques, i.e., the identification of parameters $\bar{\theta}_i$ and $\Delta\theta_i$ in Eq. (23). However, this is not pursued here for brevity, since our objective is to investigate how gPC operates for uncertainty propagation in complex cardiac models. For algorithm clarification, we have also conducted experiments assuming the parametric uncertainty follows a uniform distribution. Due to space limitation, the results of uniformly distributed uncertainty are briefly summarized in *Appendix C* with simulation results at the channel and cell levels. To calculate the Sobol SI, the MC simulations-based method proposed by Satelli [39] was adopted, where 4000 samples are randomly generated from the predefined distribution. The corresponding model outputs are then calculated and used to evaluate the main effect and the total effect of each parameter on the model outputs.

3.2.2. Cell

To identify the most sensitive parameters at the cell level, the action potential duration (APDs) at a 75% (APD_{75}) and a 90% (APD_{90}) repolarization levels were used as the output of cell models. Model parameters in both K^+ currents were assumed to be normally distributed and the mean value equals to the nominal value given in Table 2. In addition, two different levels of random variations, following the descriptions as given in previous section, i.e., a 5% and a 10% change, were used in the simulations. MC simulations with 10,000 samples were performed to evaluate the main effect and the total effect of each parameter on the model outputs.

3.3. Uncertainty propagation in ventricular cell

The uncertainties in ion channels can be propagated onto a ventricular cell, which can affect the membrane potentials at the cellular level. The gPC approximation and Galerkin projection were used in the mouse ventricular cell model (Eq. (13)) explained in Section 2.2.2 for algorithm clarification, and the gPC coefficients of AP were solved numerically using built-in function *ode15s* in MATLAB. A 0.5 ms −60 pA/pF stimulus current with a frequency of 5 Hz was used to trigger the depolarization in this work. During the experiments, it was found that, on average, after approximately 10 stimulations of APs, the changes in the AP waveform between two consecutive simulations are negligible, which means the cell has reached the steady state. Thus, data after the first 10 simulations were collected for subsequent analysis as previously reported [8]. Variabilities in AP, AP durations (APDs), and time to peak were quantified by sampling from the analytical description of the AP.

3.4. Uncertainty propagation in cardiac tissue

We further simulated the electrical propagation in 1D cell string and 2D tissue in the presence of uncertainties. For the 1D experiments, 100 ventricular cells were connected in order to form a linear fiber with a conductance of 25 nS/pF. 0.01 cm spatial resolution and 0.0001 ms temporal resolution were used. A 0.5 ms rectangular current with an amplitude of 300 pA/pF and a frequency of 5 Hz was used to one end of the cable to initiate the electrical wave propagation. It is important to note that the variabilities in cells at the cable/tissue level were considered by introducing uncertainties among cells with random variable ξ, which can quantify the variabilities among parameters in individual cells. In the 1D cable experiments, *APDs*, *Time to Peak*, and *Conduction Velocity* are measured in order to show the effects of uncertainty on the electrical conduction in 1D cable. In the 2D experiments, a small section of ventricular tissue was modeled by connecting cells (100, ×100 cells) in a uniform way to form an isotropic tissue, where the conductance was set to be 25/8 nS/pF in all directions. A fixed time step of 0.0001 ms was used in the temporal domain, and spatial step was set to 0.02 cm. The spiral wave propagation in the 2D tissue was investigated. In the presence of uncertainty, the wave contour and its variance, the tip trajectory of the spiral wave and its boundaries were identified and shown in the Results section below. To generate a spiral wave, a 0.5 ms 300 pA/pF stimulus was first applied to the left side of the tissue. When the plane-wave arrives the middle of the tissue, a second stimulus was given to the left-bottom corner, which covers one half of the tissue's width and length. Computer experiments were performed with MATLAB on a windows 7 64-bit machine.

3.5. Monte-Carlo simulations

The accuracy of the gPC-based uncertainty propagation was validated with MC simulations, where the results obtained with both gPC and MC were compared in terms of computational efficiency across different organizational levels. (1) *Ion Channel*: For each parametric uncertainty, 10,000 samples were generated from *a prior* distribution, i.e., a normal distribution with a mean value equals to the nominal values given in Table 2 and two different standard deviations (i.e., a 5% variation and a 10% variation around the mean value, respectively). For each sample, simulations were performed following the voltage clamp protocols described in Section 3.1. The mean value and the variance of the SSA and SSI of the two K^+ currents, i.e., I_{Kto}, and I_{Kur}, were calculated and compared with the results obtained using the gPC model, respectively. In addition, the computation time of MC simulations and gPC model was also recorded and compared for each K^+ current (2) *Ventricular Cell*: Samples (i.e., 10,000 samples) were randomly drawn from the input uncertainty in ion channels, and simulations were conducted with each of these samples to generate the AP of ventricular cell using models given in Section 2.2.2. Experiments were performed using built-in function *ode15s* in MATLAB, and the computation time was recorded and compared with the gPC model.

4. Results

4.1. Sensitivity analysis

4.1.1. Ion currents

As discussed in previous sections, cardiac models involve a great number of parameters. The identification of significant parametric uncertainty can potentially reduce the computational cost, thus improving the efficiency of uncertainty propagation for multiscale modeling. In this study, we first performed the variance-based sensitivity analysis to evaluate the impact of the model parameters in each K^+ current on its model outputs of SSA and SSI, respectively. The SI of the parameters are displayed in Fig. 1 with *bar-plots*. These parameters are sorted in a decreasing order with respect to their corresponding main SI. The nominal value of each parameter used in this work is given in Table 2 in Section 2.

The parameter sensitivity was investigated at two levels of variations, i.e., 5% and 10% changes around the nominal values given in Table 2, respectively. The sensitivity analysis results are shown in Fig. 1, where the two different variations (5% and 10%) show consistent results. For example, as shown in Fig. 1 (a), both the main SI and the total SI indicate that the 3rd parameter, p_3, is the most sensitive parameter of SSA in I_{Kto}. Similarly, as seen in Fig. 1 (c), p_{10} was identified as the most significant parameter of SSI in I_{Kto} in both bar-plots. For the I_{Kur} current, the most significant parameters of SSA and SSI are p_{13} and p_{15} (see Fig. 1 (b) & (d)), respectively. Thus far, we have identified the most significant parameters in each K^+ current, i.e., (p_3, p_{10}) in I_{Kto}, and (p_{13}, p_{15}) in I_{Kur}. It is worth mentioning that we assumed that parametric uncertainties among different currents are

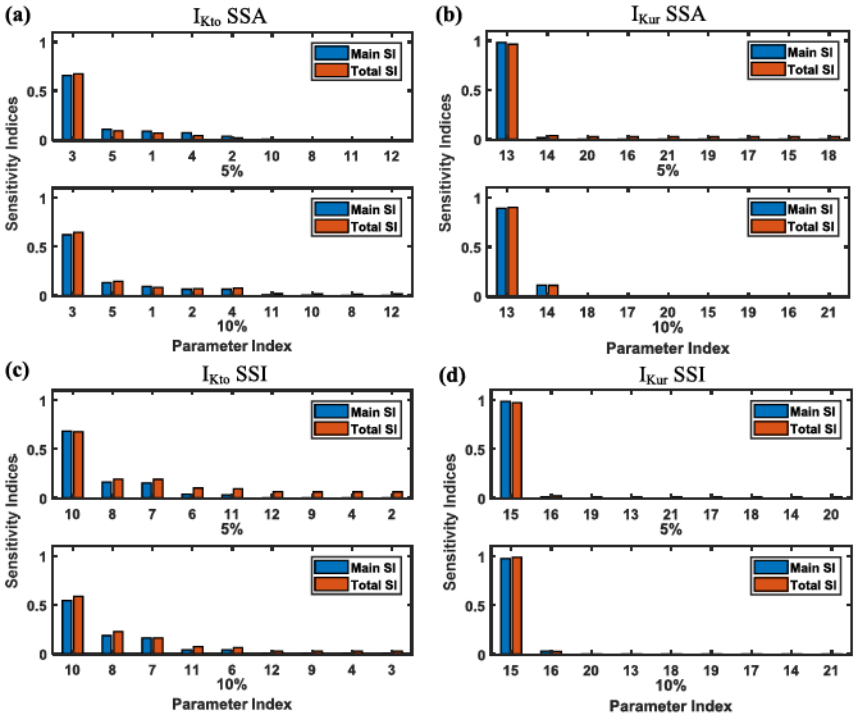

Fig. 1. SI of model parameters for SSA and SSI of I_{Kto} (a&c) and I_{Kur} (b&d).

independent, thus we investigated each type of K^+ current independently in the sensitivity analysis. Based on the sensitivity analysis results, only uncertainty in these most significant parameters is considered, which will be further propagated onto the ion channel gating and ion currents as discussed in Section 4.2.

4.1.2. Ventricular cell

Following the same procedure as done in the channel level, sensitivity analysis was performed at the cell level to identify the significant parametric uncertainty in I_{Kur} and I_{Kto} models that has larger impacts on the APDs in ventricular cell. Fig. 2 shows the main and total SIs of APD_{75} and APD_{90}, where random perturbations in each parameter follow the same probability distribution as described in Section 4.1.1.

As seen in Fig. 2, for both case studies with variations of a 5% change and a 10% change in the model parameters, the SI identifies the same set of sensitive parameters, i.e. p_3, p_4 in I_{Kto}, p_{13}, p_{18} in I_{Kur}. Based on the sensitivity analysis results, parametric uncertainty was first introduced into these 4 parameters, which will be further propagated onto Action Potential (AP), as well as electrical wave propagation in cardiac tissue.

4.2. Uncertainty propagation in ion channels

As discussed in Section 4.1, both I_{Kto} and I_{Kur} models have two significant stochastic parameters. Each parameter was further represented as a function of a random variable ξ following the procedure explained in Section 2.1, i.e., $p = \sum_{k=0}^{q} \hat{p}_k \Phi_k(\xi)$, where ξ follows a standard normal distribution, and Hermite polynomial basis function was used. Note that the gPC coefficients $\{\hat{p}_k\}$ of each parameter were determined to ensure that p follows *a prior* known normal distribution. The probability distribution of each parameter follows the same description as given in Section 4.1.1, i.e., the mean value of each parameter was set to be the corresponding nominal value in Table 2, while two different sets of variation were used in this work, i.e., a 5% variation and a 10% variation around the mean values, respectively. It is important to note that the distribution for parameters was presumed in this study to investigate the performance of the gPC-based uncertainty propagation. Uncertainty quantification methods can be used to estimate the mean and variance of parametric uncertainties from *in-vitro* data, which is not discussed here for brevity.

Since model parameter is approximated with gPC, the model prediction can be consequently estimated with gPC following the

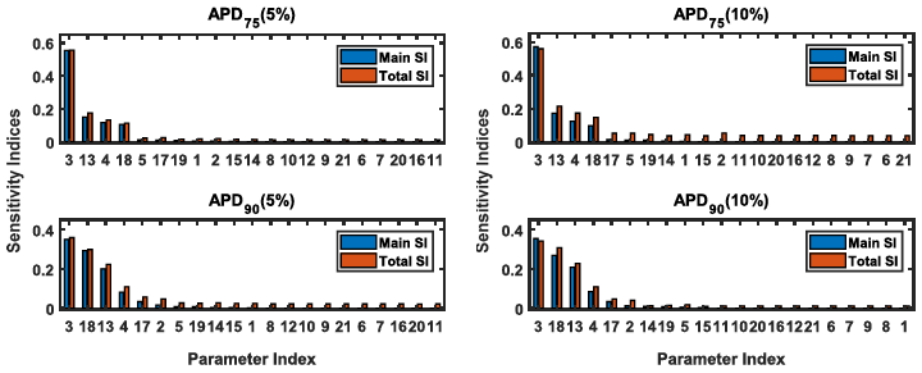

Fig. 2. SI of model parameters of K^+ channel models for APDs.

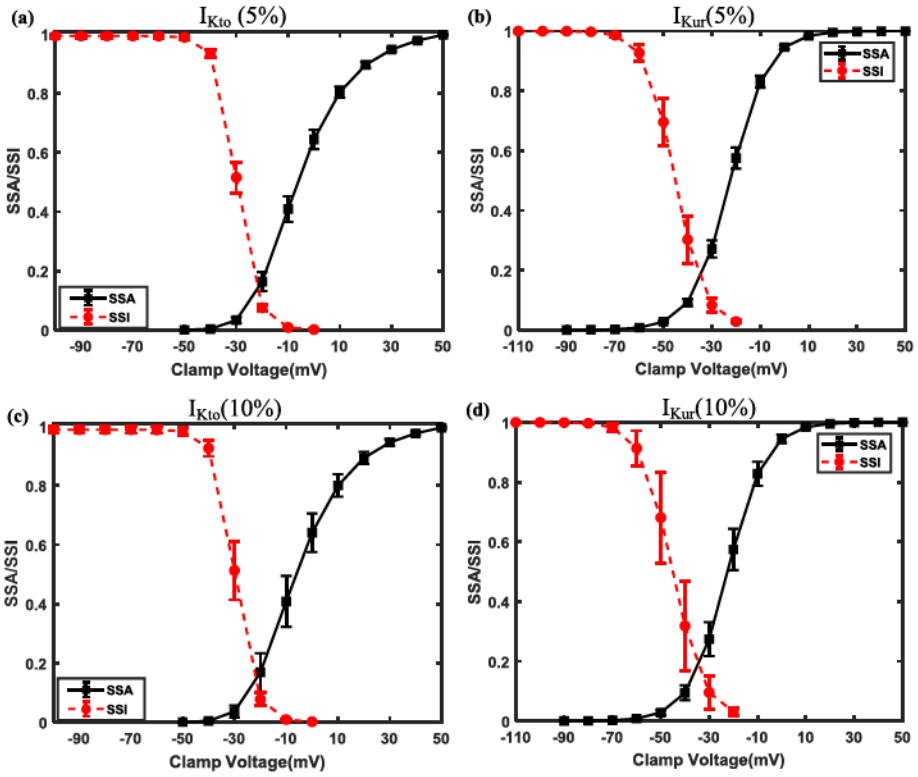

Fig. 3. Steady state activation and inactivation of I_{Kto} (a&c) and I_{Kur} (b&d).

procedures as discussed in Section 2.1. The activation gating variable a_{to} will be used as an example to illustrate how the gPC-based uncertainty propagation operates in this work. We first rewrite the parameter p_3 and the gating variable a_{to} as: $p_3 = \sum_{k=0}^{1} \hat{p}_{3,k}\Phi_k(\xi_1)$ and $a_{to} = \sum_{k=0}^{1} \hat{a}_{to,k}\Phi_k(\xi_1)$, respectively. These two approximations can be substituted into the model of a_{to} as shown in Table 1. Following this, the Galerkin projection can be used to calculate the gPC coefficients of $\{\hat{a}_{to,k}\}$. Once the gPC coefficients of a_{to} are available, the analytical expression of gating variables a_{to} can be obtained and its statistical moments at each time instant can be easily estimated with Eqs. (9) and (10) in Section 2.1. Thus far, the parametric uncertainty in p_3 has been propagated onto the gating variable a_{to} through the ion channel model. Similar procedures can be applied to other gating variables, such as i_{to}, a_{ur}, and i_{ur}, to evaluate the effect of uncertainty on model predictions in ion channel gating. Simulations were conducted using the resulting stochastic models following the experimental protocols as explained in Section 3.1, and the results are shown in Fig. 3. It is important to note that two terms are used in the gPC approximation of parametric uncertainty, the detailed discussion about the effect of the truncation on uncertainty propagation is provided in *Appendix D*.

In Fig. 3, the dynamic ranges of SSAs and SSIs for both K^+ currents at different testing voltages are given, i.e., the mean value plus or subtract the variability approximated from Eq. (10). As can be seen, the variances are relatively larger around the half-activation voltage, (i.e., -20 mV–10 mV in SSA of I_{Kto} (see Fig. 3 (a&c) black curve), and -30 mV $\sim$ -10 mV in SSA of I_{Kur} (see Fig. 3 (b&d) black curve)), and the half-inactivation voltage (i.e., -30 mV $\sim$ -20 mV in SSI of I_{Kto} (see Fig. 3 (a&c) red curve), and -60 mV $\sim$ -30 mV in I_{Kur} (see Fig. 3 (b&d) red curve)). The possible reason is that the gating of the K^+ channels is more active in these voltage ranges, and slightly variations in model parameters can lead to significant changes in the gating activities. In addition, it was found that the increase of uncertainty in model parameter can result in larger variations in model predictions. For example, as seen in Fig. 3, the variances in SSA and SSI of both I_{Kto} and I_{Kur} are larger, when the variance of the parametric uncertainty is set to a 10% change around the mean value, as compared to a 5% change near the mean value (see Fig. 3 (a) *vs* Fig. 3 (c) and Fig. 3 (b) *vs* Fig. 3 (d)).

To validate the experimental results and to show the efficiency of gPC-based uncertainty propagation, MC simulations were used in this work. For both gPC and MC, the upper bounds and the lower bounds of the steady state activation and inactivation of I_{Kto} are shown in Fig. 4. Note that these two bounds for gPC and MC were estimated using *2-fold* standard deviation. As can be seen, the results obtained with both gPC and MC can converge to the same upper and lower bounds, which verifies the accuracy of the gPC. However, it was found that MC demands more simulation runs to obtain the similar results as compared to gPC.

For comparison purpose, we quantitatively measured and compared the performance of gPC and MC in terms of the computation time and accuracy. The results are summarized in Table 3. As can be seen in Table 3, the gPC and MC can provide similar results at different clamp voltages, i.e., similar estimations of mean and standard deviation in model predictions in the presence of parametric uncertainty. However, there is significant difference between gPC and MC in terms of the computation time. The gPC only requires one simulation run to estimate the mean and variance in the model prediction, but MC may demand thousands of simulation-runs to obtain the similar results as gPC. The computation time required by gPC and MC for accurate estimations of the mean and variance of model predictions for both SSAs and SSIs are given in Table 3. As seen in the last two columns, the gPC only requires about 1 s to generate the upper and lower bounds. However, MC simulations require approximately 47–144 min to obtain similar results. Note that 10,000 samples were used for MC simulations in this work. In addition, it was found that the computational burden of MC can be decreased when a small number of samples were used, but the accuracy was sacrificed. Additionally, we compared the mean and standard deviation of SSA and SSI for both K^+ currents with a 5% and a 10% variation in parametric uncertainty, respectively. As listed in Table 3, the increased variation (i.e., from 5% to 10%) in model parameters can lead to a larger variance in the model predictions of SSA and SSI.

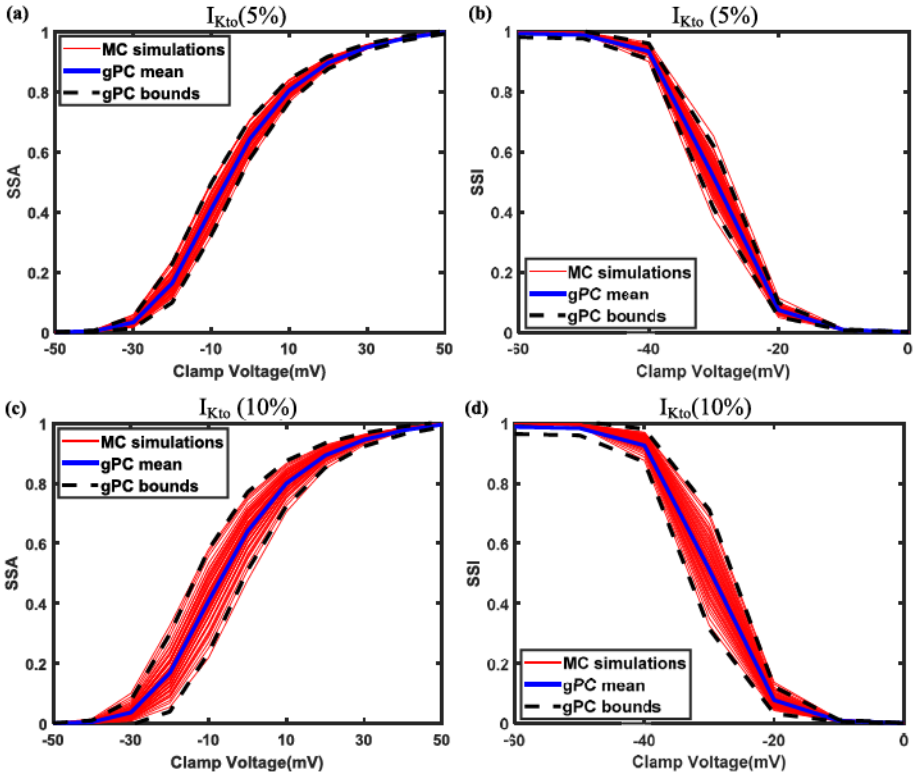

Fig. 4. Comparison between gPC and MC Simulation. ((a&c) Upper bound and Lower bound of Steady State Activation of I_{Kto}, (b&d) Upper bound and Lower bound of Steady State Inactivation of I_{Kto}).

Table 3
Summary of comparison results (MC *vs.* gPC).

Currents	Standard deviation	Methods	SSA			SSI			Computation Time (s)	
			−20 mV	−10 mV	0 mV	−40 mV	−30 mV	−20 mV	SSA	SSI
I_{Kto}	5%	gPC	0.163 ± 0.032	0.408 ± 0.043	0.644 ± 0.033	0.935 ± 0.013	0.516 ± 0.052	0.075 ± 0.012	0.631	1.310
		MC	0.163 ± 0.032	0.409 ± 0.043	0.644 ± 0.033	0.935 ± 0.013	0.516 ± 0.052	0.075 ± 0.012	6598.009	8659.850
	10%	gPC	0.168 ± 0.065	0.408 ± 0.086	0.640 ± 0.065	0.926 ± 0.027	0.513 ± 0.099	0.077 ± 0.022	0.625	1.221
		MC	0.168 ± 0.064	0.408 ± 0.084	0.640 ± 0.065	0.925 ± 0.028	0.513 ± 0.100	0.078 ± 0.026	6598.143	8659.951
			−30 mV	−20 mV	−10 mV	−50 mV	−40 mV	−30 mV		
I_{Kur}	5%	gPC	0.271 ± 0.029	0.575 ± 0.035	0.831 ± 0.020	0.696 ± 0.081	0.302 ± 0.078	0.083 ± 0.025	0.546	0.710
		MC	0.271 ± 0.027	0.575 ± 0.033	0.831 ± 0.019	0.696 ± 0.082	0.302 ± 0.079	0.083 ± 0.026	2804.161	5690.349
	10%	gPC	0.274 ± 0.057	0.574 ± 0.069	0.828 ± 0.040	0.681 ± 0.151	0.318 ± 0.149	0.096 ± 0.056	0.532	0.712
		MC	0.274 ± 0.057	0.574 ± 0.069	0.828 ± 0.041	0.681 ± 0.154	0.318 ± 0.151	0.096 ± 0.061	2803.833	5691.034

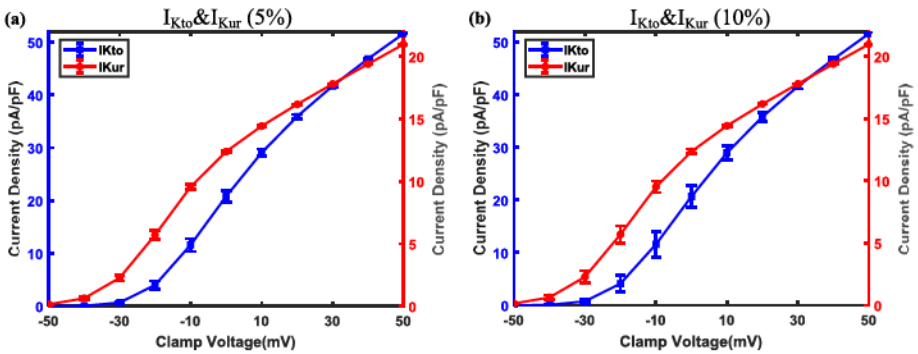

Fig. 5. Current density of I_{Kto} and I_{Kur}.

Table 4
Current density.

Currents		−30 mV	−20 mV	−10 mV	0 mV	10 mV	20 mV	30 mV
I_{Kto}	5%	0.673 ± 0.200	3.995 ± 0.787	11.580 ± 1.232	20.770 ± 1.055	29.060 ± 0.687	35.890 ± 0.410	41.660 ± 0.255
	10%	0.745 ± 0.420	4.121 ± 1.583	11.590 ± 2.448	20.670 ± 2.103	28.950 ± 1.362	35.800 ± 0.820	41.590 ± 0.484
I_{Kur}	5%	2.262 ± 0.239	5.706 ± 0.348	9.550 ± 0.231	12.380 ± 0.093	14.430 ± 0.031	16.160 ± 0.010	17.790 ± 0.003
	10%	2.285 ± 0.474	5.695 ± 0.687	9.517 ± 0.463	12.360 ± 0.190	14.420 ± 0.063	16.160 ± 0.020	17.790 ± 0.006

We also investigated the stochasticity in the current density of I_{Kto} and I_{Kur} in the presence of parametric uncertainty. These two currents can be approximated with gPC expansion as:

$$IKto = G_{to}\left(\sum_{k=0}^{1}\hat{a}_{to,k}\Phi_k(\xi_1)\right)^3\left(\sum_{k=0}^{1}\hat{i}_{to,k}\Phi_k(\xi_2)\right)(V-E_K), \tag{24}$$

and

$$IKur = G_{ur}\left(\sum_{k=0}^{1}\hat{a}_{ur,k}\Phi_k(\xi_3)\right)\left(\sum_{k=0}^{1}\hat{i}_{ur,k}\Phi_k(\xi_4)\right)(V-E_K), \tag{25}$$

where ξ_1 and ξ_2 are two random variables that were used to approximate perturbations in parameters p_3 and p_{10} in the I_{Kto} model, ξ_3 and ξ_4 are two random variables used to approximate variation in parameters of p_{13} and p_{15} in the I_{Kur} model. These gPC coefficients, i.e., $\{\hat{a}_{to,k}\}$, $\{\hat{i}_{to,k}\}$, $\{\hat{a}_{ur,k}\}$, and $\{\hat{i}_{ur,k}\}$, can be calculated following the procedures as explained in Section 2.1. Based on the analytical expressions of K^+ currents, we further investigated the $I-V$ relationships. The simulation results are shown in Fig. 5. As can be seen, the ion currents of I_{Kto} and I_{Kur} exhibit larger variations, when the clamp voltages are between -20 mV–10 mV for I_{Kur} and -20 mV ~ -10 mV for I_{Kto}, respectively. In addition, by comparing Fig. 5 (a) and Fig. 5 (b), it was found that the increase of standard deviation, i.e., from a 5% change to a 10% change, can introduce more variation in both K^+ currents. For clarity, the uncertainty in the current densities resulting from parametric uncertainty is summarized in Table 4, along with their corresponding mean values at each clamp voltage.

4.3. Uncertainty propagation in cardiac cell

In cell level, we introduced uncertainty (i.e., a 5% variation and a 10% variation) into the sensitive parameters of p_3, p_4 in I_{Kto}, and p_{13}, p_{18} in I_{Kur}, identified from sensitivity analysis (see section 4.1.2), which results in uncertainty in ion channel models. Note that parametric uncertainty may originate from *cell-to-cell* variability. Such uncertainty can be further propagated onto AP through the cell model described in Section 2.2.2. Using the stochastic gPC models of I_{Kto} and I_{Kur}, it is possible to approximate the AP with a gPC expansion as: $V=\sum_{k=0}^{4}\hat{V}_k\Psi_k(\xi)$, for which the coefficients can be similarly solved as done for the channel models. Given the analytical expression of the AP, we can easily determine the uncertainty in quantities such as APDs and AP peak, which are previously used in various studies in order to gain insights of cardiac arrhythmia vulnerability [32]. Simulations of cardiac cells follow the design procedures as described in Section 3.3, i.e., a 0.5 ms stimulus current with a magnitude of 60 pA/pF and a frequency of 5 Hz was used to trigger the depolarization. When the changes in the AP waveform between two consecutive stimulations are negligible, i.e., after approximately 10 stimulations, data were collected for uncertainty quantification.

Fig. 6 shows the uncertainty in AP, resulting from parametric uncertainty for two different case studies, i.e., a 5% change in parameter around the nominal value and a 10% change in the vicinity of the nominal value. As shown in Fig. 6, the variation in AP with a 10% change is larger than the 5% change. In addition, for both case studies, it was found that the variation in AP in the repolarization period, i.e., 1825 ms–1850 ms, is larger than the rest periods such as upstroke and resting states. This is because both K^+ currents (I_{Kto} and I_{Kur}) mainly contribute to the repolarization of AP. For comparison, we further quantified the shape of AP with APD_{25}, APD_{50}, APD_{75}, APD_{90}, peak value, and time to peak (TTP). The means and the standard deviations of these quantities are summarized in Table 5. As seen in Table 5, these quantitative measures show that the standard deviations in APD_{75} and APD_{90} are larger than APD_{25} and APD_{50} for both 5% and 10% variations. In addition, it was found that uncertainty in K^+ channel models has little impact on the peak value and TTP of AP, since the relative variations in the peak value and the TTP of AP are less than 1% and 0.3%, respectively.

To validate the results obtained with gPC, computer experiments with MC were conducted and the results are shown in Fig. 6. As seen, the red lines in Fig. 6 represent the APs generated with MC, whereas the blue and black lines are the mean, lower and upper bounds calculated with gPC. The APs generated with MC are bounded by the upper and lower bounds calculated with the gPC, which verifies the accuracy of gPC. Again, these two bounds of gPC were estimated using *2-fold* standard deviation. We also compared the efficacy in terms of computation time for both gPC and MC. It was found that the computation time of the gPC is not affected by the level of uncertainty in parameters and can provide the lower and upper bounds in one simulation run,

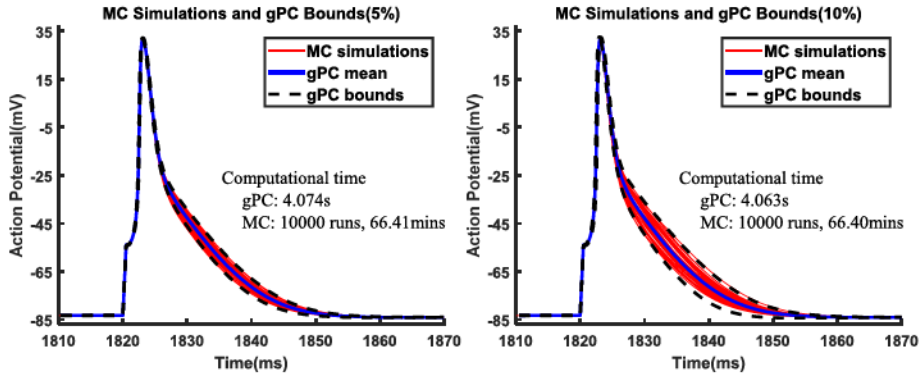

Fig. 6. Mean, upper, and lower bounds of AP obtained with gPC and MC.

Table 5
Summary of uncertainty in APDs and AP peak.

Standard deviation	APD_{25} (ms)	APD_{50} (ms)	APD_{75} (ms)	APD_{90} (ms)	Time to Peak (ms)	Peak (mV)
5%	1.967±0.077	4.029±0.157	12.976±0.600	20.000±0.863	3.121±0.007	31.937±0.145
10%	1.971±0.142	4.043±0.311	12.984±1.161	20.080±1.643	3.151±0.009	31.800±0.281

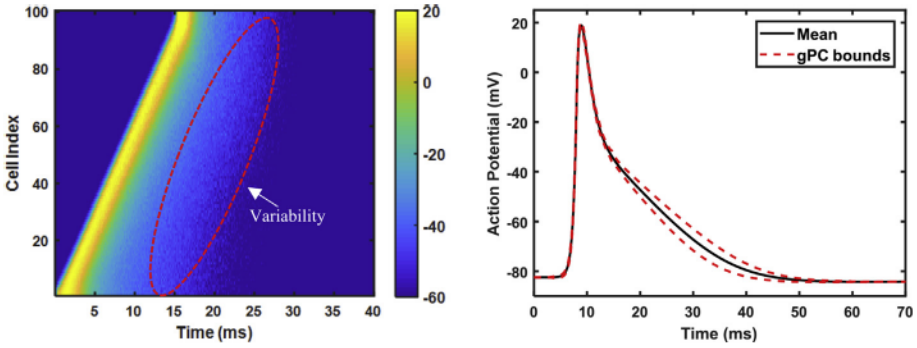

Fig. 7. (a) Electrical propagation in 1D cable, and (b) Mean, upper, and lower bounds of AP in 1D cable.

which takes on average about 4 s. In contrast, the MC requires more than 66 min for 10,000 simulation runs, where 10,000 samples were generated for $\xi = \{\xi_1, \xi_2, \xi_3, \xi_4\}$ that are used to approximate the most significant parameters identified in Section 4.1. It should be noted that the computational cost can be reduced when a smaller number of samples of ξ were used in MC, but the accuracy would be sacrificed. This shows the efficiency of the gPC method, thereby demonstrating its advantage for uncertainty propagation in ion channel and cardiac cell models.

4.4. Uncertainty propagation in 1D cable and 2D tissue

We further investigated the performance of gPC-based uncertainty propagation on 1D cell string and 2D tissue. In this case study, ventricular cells were connected with gap junctions in order to form a 1D cable and a 2D cell array. For the 1D cable experiment, stimulations were applied to the left of the cable to initiate the excitation, and the electrical waves were generated and propagated from one end to the other. Note that we propagated the parametric uncertainty in K^+ channel models onto each cardiac cell in 1D cable to account for cellular variabilities, which was introduced through random variables ξ. Based on the methodology described in Section 2.1, the AP of each cell in the 1D tissue can be approximated with a gPC approximation, i.e., $V_i = \sum_{k=0}^{4} \hat{V}_{i,k}\Psi_k(\xi), i = 1, 2, \ldots, 100$, which will further be substituted into the 1D cable model given in Section 2.2.3. By applying Galerkin projection to the models of the 1D cable and by solving the integral with Sparse Quadrature rule, we can approximate the mean value $\mathbb{E}(V_i)$ and the corresponding variance $\mathbb{V}(V_i)$ of AP for each cell with gPC models. Fig. 7 shows the electrical propagation on 1D cable (Fig. 7 (a)), and the upper and lower bounds of the APs in the cable (Fig. 7 (b)).

As seen in Fig. 7 (a), the horizontal axis represents the propagation time while the vertical axis shows the cell index. Different colors indicate different values of AP. Variabilities can be observed among the repolarization of cells, which is consistent with the observations in the cell level, i.e., parametric uncertainty in K^+ currents of I_{Kto} and I_{Kur} can lead to variations in repolarization. Further, Fig. 7 (b) shows the mean, upper, and lower bounds of the APs measured in the 1D cable. To quantify the variations in the 1D cable, we further investigated the APDs, Peak, and TTP. The mean values and variance in these quantities were calculated from the cable and the results are summarized in Table 6.

As can be seen in Table 6, APD_{75} and APD_{90} appear larger variations, as compared to APD_{25} and APD_{50}. Additionally, it was found that the uncertainty in K^+ channels has little effect on the peak values and the TTPs. We further quantified the conduction velocity (CV) as shown in Table 6, which was calculated using the distance between the 21st and 80^{th} cell divided by the travelling time of the wavefront between these two cells. As seen, the maximum and minimum values of the CV are 0.647 m/s and 0.645 m/s, respectively. In terms of computation time, it was found that on average about 125.90 min were required for a 100 ms simulation with the gPC on a windows 7 64-bit desktop.

In addition, 100 × 100 cell array was constructed in order to study the electrical propagation on two-dimensional tissue. Similarly, following the methodology presented in Section 2.1, the AP of each cell in the 2D tissue was approximated as: $V_{i,j} = \sum_{k=0}^{1} \hat{V}_{i,j,k}\Psi_{i,j,k}(\xi), i = 1, 2, \ldots, 100, j = 1, 2, \ldots, 100$, which can be substituted into the 2D tissue model described in Section 2.2.3. The uncertainty in AP originates from the uncertainty in K^+ channels. Using Galerkin projection, the model can be transformed into a set of coupled equations of gPC coefficients $\hat{V}_{i,j,k}$, which can be solved numerically through Sparse Quadrature and

Table 6
Measurements of 1D cable.

APD_{25} (ms)	APD_{50} (ms)	APD_{75} (ms)	APD_{90} (ms)	Time to Peak (ms)	Peak (mV)	CV(m/s)		Running time (mins)/(100 ms)
						min	max	
2.740±0.019	6.303±0.265	17.222±1.743	26.402±2.842	5.58±0.010	18.927±1.227	0.645	0.647	125.90

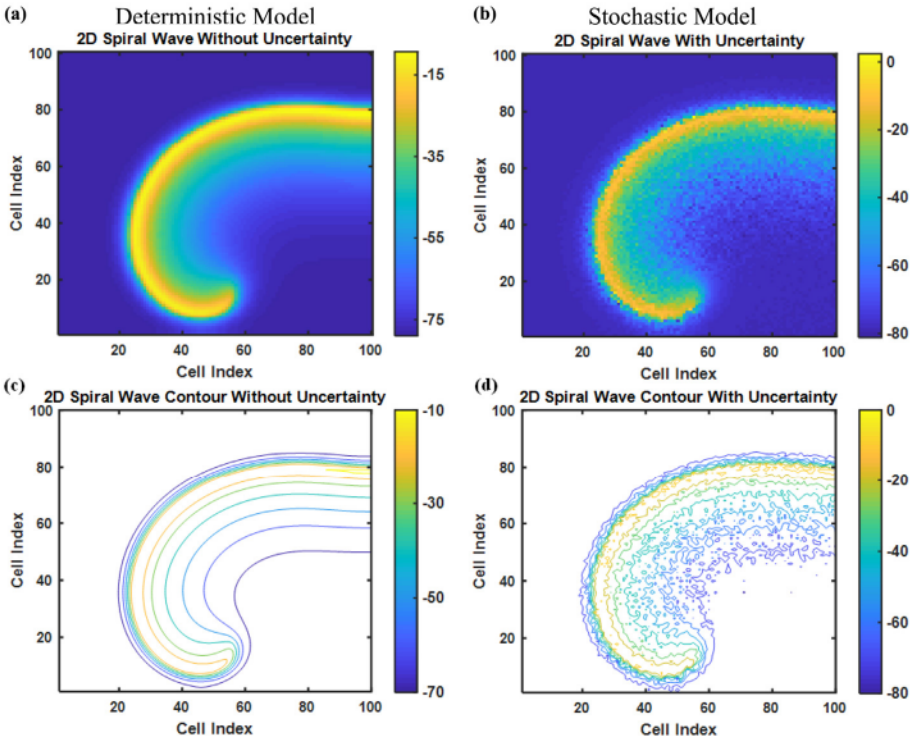

Fig. 8. Spiral waves and their contour plots modeled with deterministic model (a & c) and gPC model (b & d).

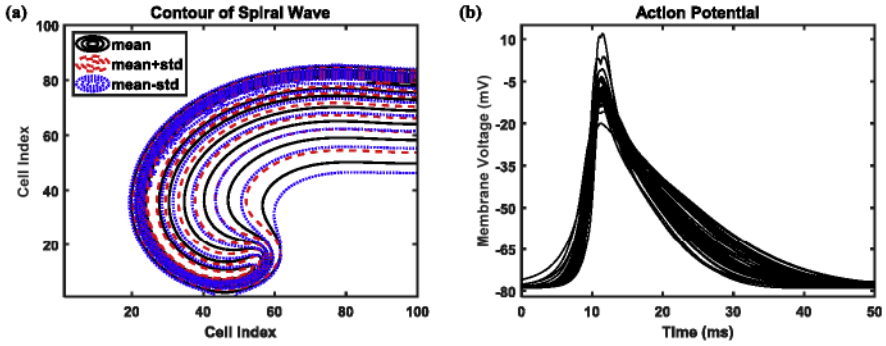

Fig. 9. (a) Contour plots of spiral wave with gPC model and (b) APs of 20 cells in the 2D tissue.

finite difference method. Once the gPC coefficients are available, we can easily approximate the mean value $\mathbb{E}(V_{i,j})$ and the variance $\mathbb{V}(V_{i,j})$ of APs in the 100 × 100 cell array. For comparison, Fig. 8 shows the results of spiral waves of the 2D tissue modeled with both deterministic model and gPC model, respectively.

For clarity, the spiral waves in Fig. 8 were visualized as images with different colors representing different values of membrane potentials. As seen in Fig. 8 (a) and (c), deterministic model can provide fixed predictions of membrane potential, which may fail to incorporate cell variabilities. However, as shown in Fig. 8 (b) and (d), the spiral wave obtained with the gPC model can account for variabilities among cells. It is worth mentioning that large variations appear in the wave tails (i.e., repolarization phase of APs). This is because parametric uncertainties in both K^+ currents of I_{Kto} and I_{Kur} were considered in this work, and these two currents contribute greatly to the repolarization of a single AP cycle. In the presence of uncertainty, the gPC model can provide a more realistic description of ventricular tissue activities, since it can account for the *cell-to-cell* variabilities.

To quantify the uncertainty in the 2D tissue, Fig. 9 shows the contours of the spiral wave and its confidence intervals as well as the APs of different cells on the 2D tissue for the first 50 ms. As seen in Fig. 9 (a), the solid black lines show the mean value of the contours, while the red and blue dash lines show the lower and upper bounds associated to the mean values. In Fig. 9 (b), the APs of 20 random selected cells on the 2D tissue for the first 50 ms are plotted. The spiral wave leads to variations in AP among different cells, and the repolarization shows larger variations due to the parametric uncertainty in the K^+ currents of ion channel models.

In addition, we studied the evolution of the tip of the spiral wave on the 2D tissue. The tip trajectory was tracked following the method proposed by Gray et al. [40], in which a cardiac phase variable for each cell can be defined as:

$$\theta_{i,j}(t) = arctan\left(\frac{V_{i,j}(t+\tau) - V_{ref}}{V_{i,j}(t) - V_{ref}}\right), \tag{26}$$

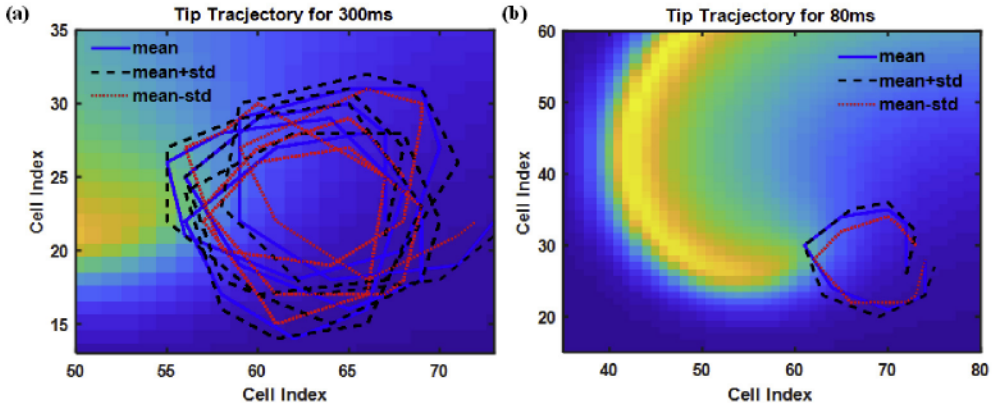

Fig. 10. Tip trajectory (a) 400 ms and (b) 80 ms

where V_{ref} and τ are threshold parameters, which were set as -70 mV and 10 ms in this work, respectively; *arctan* is the inverse of the tangent function. Given the phase variable, the line integral was numerical calculated as:

$$\oint \nabla\theta \cdot dl, \tag{27}$$

where l is the coordinates of 8 neighbor cells. The tip was determined as the location that a phase singularity is present.

Fig. 10 (a) shows the mean, upper and lower bounds of the tip trajectory for 400 ms, where the blue solid line is the mean trajectory, and the black dash line and the red dot line are the lower and upper bounds. For better illustration, tip trajectory for 80 ms was shown in Fig. 10 (b). As seen, the progression of the wave tip stabilized in the area between the upper bound and lower bound.

5. Discussions

This paper investigated the gPC-based uncertainty propagation for multi-scale cardiac modeling. It has demonstrated the potential of gPC for efficient uncertainty propagation in cardiac ion channels, cell, 1D cable, and 2D tissue. The variance decomposition-based sensitivity analysis was first used to identify the most significant parametric uncertainty, which was further approximated with polynomial functions of random variables from the Wiener-Askey framework, and then propagated onto K^+ channel gating and ion currents of I_{Kto} and I_{Kur}. The uncertainty in ion channel level was further propagated onto the AP of mouse ventricular cell in a computationally efficient fashion. The computation time for gPC models and MC simulations was compared at ion channel level and cellular level. The simulation results show that gPC is superior to MC in terms of computational efficiency. In addition, uncertainty was further propagated onto 1D cable and 2D tissue with the gPC method, and conduction velocity and spiral wave propagation were measured to show the performance of the gPC method.

5.1. Monte Carlo Simulations vs gPC

Sampling-based techniques such as MC simulations are one of the most popular methods for uncertainty analysis [7,17]. The key idea of MC is to first generate a set of random samples from *a prior* probability distribution, and then perform simulations with each of these samples. The simulation results are used to evaluate the effect of parametric uncertainty on model predictions. The performance of MC greatly depends on the number of samples used in MC simulations. For complex models involving a large number of equations, MC method can be computationally prohibitive. The gPC method, however, can approximate the uncertainty as a function of random variables and analytically propagate the uncertainty onto model predictions. In this way, the variability in model predictions can be easily approximated with the gPC approximation, which can significantly reduce the computational burden. As shown in the result section, the gPC can provide an accurate approximation of the upper and lower bounds of model outputs. Experimental results indicate that gPC outperforms MC at ion channel level and cellular level (see Sections 4.2 and 4.3). In addition, gPC can be applied to 1D cable and 2D tissue to quantify *cell-to-cell* variability, which was found be to be inefficient with MC method due to the heavy computational cost, as previously reported [41]. The current study verified the feasibility of gPC method for uncertainty propagation in multi-scale cardiac model, and has showed its superior performance as compared to MC.

It is worth mentioning that when the dimension of the random vector ξ increases significantly, the computational cost may not be trackable with gPC. As previously reported, techniques such as the adaptive sparse basis construction method [23,42] can be used to improve the computational efficiency. However, this can only reduce the computation time to a certain degree when the dimension of random vector is high. In contrast, the convergence rate of MC is independent of the dimensionality asymptotically. Thus, when the random dimensionality becomes large enough, the MC method may be preferable. We would like to point out that the sensitivity analysis was used in this work to identify significant parametric uncertainties, which can significantly reduce the dimension of parametric uncertainty, thus improving the efficiency of gPC-based uncertainty propagation. Additionally, parametric uncertainty may be described by arbitrary random variables other than standard distributions from the Wiener-Askey family. This may affect the accuracy of gPC-based uncertainty propagation. To overcome this challenge, random variables (ξ) used to approximate uncertainty should be carefully defined and new polynomial functions can be built to satisfy the orthogonality requirement with respect to the random variables used to estimate input uncertainties [43]. The development of new polynomial functions for uncertainty quantification and propagation was reported in our previous work and it is not discussed here for brevity [44].

5.2. Randomness vs variability

The gPC method can model both randomness and variabilities in cardiac cells. APs of individual ventricular cell can be shaped by the interplay of deterministic law of cardiac cell excitation and randomness. The AP of each cell can exhibit fluctuations and uncertainty due to

the intrinsic noise. In this study, AP of a single cell was derived as a function of random vector ξ, i.e., $V_i = \sum_{k=0}^{4} \hat{V}_{i,k}\Psi_k(\xi)$, which introduces stochasticity into the deterministic model of the ventricular cell, thus quantifying the randomness in AP predictions. In addition, genetically identical cells in ventricles can have different ion currents and APs, which may lead to *cell-to-cell* variability. In this current work, each cell in the 1D cable and 2D tissue models was described with a stochastic model defined through random vector ξ. The random vector enables the gPC model the capability of capturing variabilities among cells. A salient feature of the gPC model is that it can integrate the randomness and *cell-to-cell* variability simultaneously in a unified framework.

6. Conclusions

In this paper, the gPC method is presented to propagate parametric uncertainty across multiscale cardiac models of ion channel, cell, 1D cell string, and 2D tissue. The study has demonstrated the feasibility and efficiency of gPC-based uncertainty propagation in multiscale cardiac modeling. As compared to MC simulations, the gPC shows its superior performance in term of computational efficiency. In addition, the integration of gPC with deterministic cardiac models provides a stochastic framework that can account for both randomness and variabilities in cardiovascular system, thus enabling a more reliable and robust modeling platform for knowledge discover, disease mechanism investigation, and treatment design and planning.

Conflict of interest

None Declared.

Acknowledgements

The authors would like to acknowledge the financial supports from National Science Foundation, US (CMMI-1646664, CMMI-1728338, CMMI-1727487).

Appendix A. Justification of Eq. (5)

To show the rationale of Eq. (5), we will use one example here. Suppose $n_\theta = 2$, which means there are two parametric uncertainties. Firstly, we set the highest order of the two-dimensional orthogonal polynomials as: $Q = 2$. Since the highest order of the univariate polynomials $q \le Q$, indicating that each univariate polynomial basis would just contain $\{\Phi_0(\xi_i), \Phi_1(\xi_i), \Phi_2(\xi_i)\}$. All combination of these univariate polynomials would have 9 components. However, the selection of $Q = 2$ will rule out the third and fourth order polynomials $\{\Phi_1(\xi_1)*\Phi_2(\xi_2),\ \Phi_2(\xi_1)*\Phi_1(\xi_2),\ \Phi_2(\xi_1)*\Phi_2(\xi_2)\}$, and this will further restrict the two-dimensional polynomial basis functions to be from the following combinations $\{\Phi_0(\xi_1)*\Phi_0(\xi_2),\ \Phi_1(\xi_1)*\Phi_0(\xi_2),\ \Phi_0(\xi_1)*\Phi_1(\xi_2),\ \Phi_1(\xi_1)*\Phi_1(\xi_2),\ \Phi_2(\xi_1),\ \Phi_2(\xi_2)\}$, which only involves 6 items. Therefore, $Q = 5$, which is identical to the results obtained from Eq. (5), i.e. $((2 + 2)!/(2!2!)) - 1$. In addition, as an example, Tables A1 and A2 show a few polynomial basis functions used for approximating the model response in the presence of one- and two-dimensional random variables.

$$Q = \left(\frac{(n_\theta + q)!}{n_\theta! q!}\right) - 1 \tag{5}$$

Table A1
One-dimensional polynomial chaos basis functions

i	Q^*	i^{th} polynomial basis function Ψ_i
0	0	1
1	1	ξ_1
2	2	$\xi_1^2 - 1$
3	3	$\xi_1^3 - 3\xi_1$
4	4	$\xi_1^4 - 6\xi_1^2 + 3$

*As defined in (21), Q is the order of homogenous polynomial chaos.

Table A2
Two-dimensional polynomial chaos basis functions

i	Q^*	i^{th} polynomial basis function Ψ_i
0	0	1
1	1	ξ_1
2		ξ_2
3	2	$\xi_1^2 - 1$
4		$\xi_1\xi_2$
5		$\xi_1^2 - 1$
6	3	

(*continued on next page*)

Table A2 (*continued*)

i	Q^*	i^{th} polynomial basis function Ψ_i
		$\xi_1^3 - 3\xi_1$
7		$\xi_1^2\xi_2 - \xi_2$
8		$\xi_1\xi_2^2 - \xi_1$
9		$\xi_2^3 - 3\xi_2$
10	4	$\xi_1^4 - 6\xi_1^2 + 3$
11		$\xi_1^3 - 3\xi_1\xi_2$
12		$\xi_1^2\xi_2^2 - \xi_1^2 - \xi_2^2 + 1$
13		$\xi_1\xi_2^3 - 3\xi_1\xi_2$
14		$\xi_2^4 - 6\xi_2^2 + 3$

Appendix B. The gPC-based uncertainty quantification and propagation

To demonstrate how gPC operates for uncertainty propagation, we will use the activation gating variable a_{to} of I_{Kto} as an example. The first-principle model used for a_{to} can be defined as:

$$\frac{da_{to}}{dt} = \alpha_a(1 - a_{to}) - \beta_a a_{to},$$

Suppose a parameter p_3 that can be used to define the dynamic of α_a and β_a follow a normal distribution with a mean value of 30 and a standard deviation of 3, a gPC expansion of p_3 can then be defined as below:

$$p_3 = 30 + 3\xi,$$

where $\xi \sim N(0,1)$, which is a standard normal distribution from the Askey-Wiener scheme. Since p_3 is approximated with ξ and since p_3 is related to a_{to}, a_{to} would be a function of ξ, which can be defined as $a_{to}(\xi)$. The uncertainty in a_{to} would be further propagated onto the cell membrane potential V, thus$V$ can be also defined with ξ, i.e., $V(\xi)$. In the presence of parametric uncertainty in p_3, α_a and β_a can be mathematically described as:

$$\alpha_a(\xi) = p_1\exp(p_2\,(\mathrm{V}(\xi) + p_3(\xi))),$$

$$\beta_a(\xi) = p_4\exp(p_5\,(\mathrm{V}(\xi) + p_3(\xi))),$$

As seen, parametric uncertainty in p_3 can be propagated onto the membrane potential V, which in turn introduces stochasticity in the activation gating variable a_{to}.

Based on these aforementioned gPC expansions, Galerkin projection can be used for uncertainty propagation. By setting the highest order of the resulting polynomials of a_{to} to 1, the gPC expansion of a_{to} can be explicitly defined as: $a_{to} = a_{to0} + a_{to1}\xi$. Following the procedures of the Galerkin projection, the original ODE function of a_{to} can be transformed into two coupled equations as below:

$$\frac{da_{to0}}{dt} = \int_{-\infty}^{+\infty} [\alpha_a(\xi)(1 - a_{to}(\xi)) - \beta_a(\xi)a_{to}(\xi)]\cdot p(\xi)d\xi,$$

$$\frac{da_{to1}}{dt} = \int_{-\infty}^{+\infty} [\alpha_a(\xi)(1 - a_{to}(\xi)) - \beta_a(\xi)a_{to}(\xi)]\cdot\xi\cdot p(\xi)d\xi,$$

where a_{to0} and a_{to1} are the gPC expansion coefficients that can be used to approximate the uncertainty in a_{to}. It should be noted that the resulting two coupled equations are of the same form as compared to the original model. In addition, it is possible that resulting coupled equations system does not have analytical solution due to the integration step involved in the Galerkin projection. However, this coupled equations system can be solved by numerical methods such as the sparse quadrature rules in combination with Runge-Kutta methods.

At each time instant, the coefficients a_{to0} and a_{to1} can be calculated and then used to approximate uncertainty in a_{to}, which would be further incorporated in I_{Kto}. Following this, I_{Kto} together with other currents would be applied to calculate the uncertainty in V. The function of V is a simple form ODE, for which the gPC expansion can be determined as done for a_{to}.

Appendix C. Uncertainty propagation at the channel and cell levels with uniformly distributed uncertainty

The uncertainty propagation at the channel and cell levels using uniform distribution were investigated. For algorithm verification, a 10% and a 25% variation were introduced in the sensitive parameters, respectively, and the simulation results were compared with MC simulations. These results are shown in Fig. A1 below, where the gPC method and MC simulation show consistent results, thus justifying the accuracy of the gPC approach in this work.

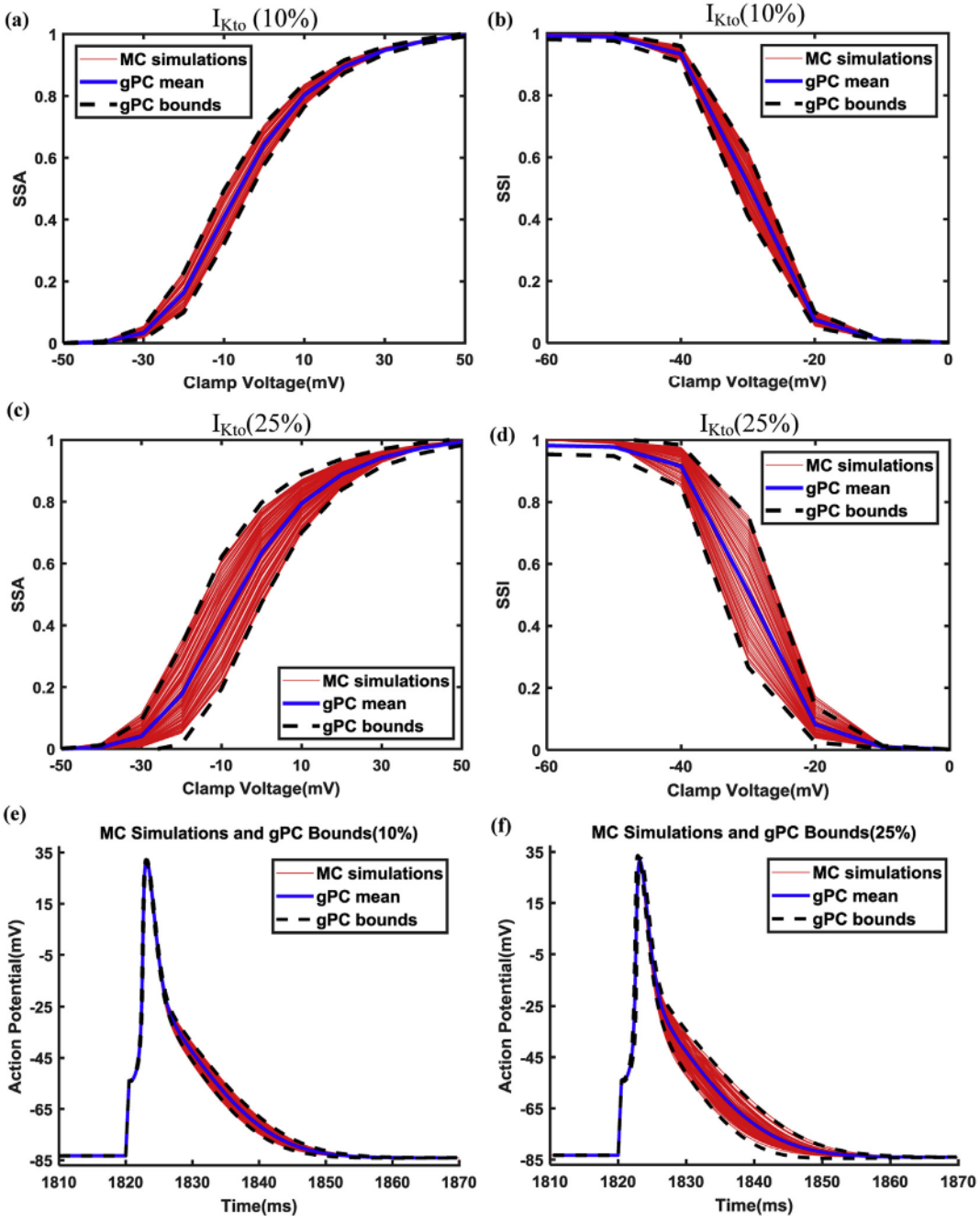

Fig. A1. Mean, upper, and lower bounds of AP obtained with gPC and MC for uniform distribution.

Appendix D. Effects of the truncation on the accuracy of the uncertainty propagation

In addition, we have tested the effect of adding more terms to the gPC expansion by setting q to 2. When q is set to 2, the approximation of the gating variable has 6 terms, i.e. $Q = 5$. However, the increase of polynomial terms does not significantly affect the results. As seen in Fig. A2 and Table A3, there is little difference in the Steady State Activation and Inactivation of I_{Kto}, when q was set to 1 and 2, respectively. Further, we investigated the effects of increasing the number of gPC expansion terms ($q = 2$) on AP in the cellular level. It was found that the mean, upper bound, and lower bound of AP estimated with $q = 2$ are very close to the results obtained using $q = 1$ (see Fig. A3), thus demonstrating that $q = 1$ is sufficient for the current simulation study.

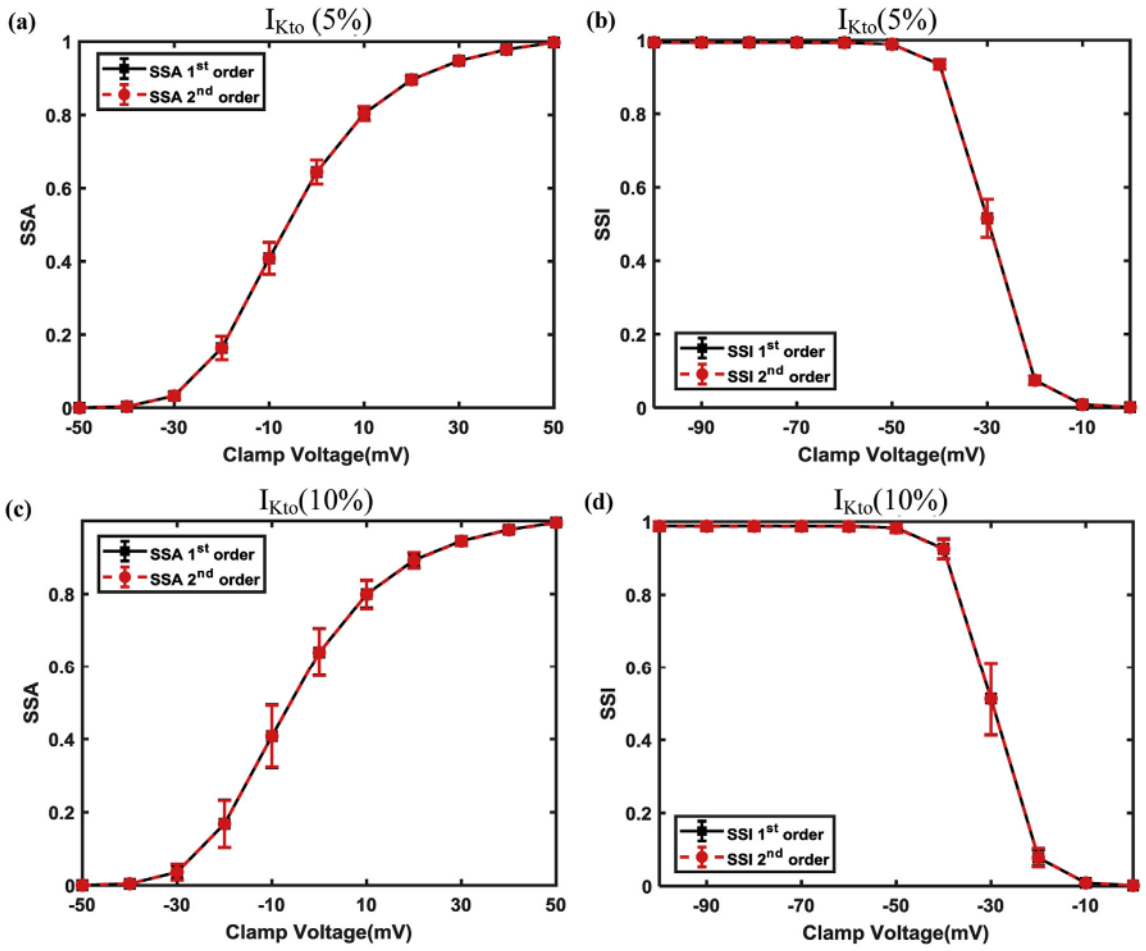

Fig. A2. SSA and SSI curve comparison by using 1st and 2nd order expansion.2

Table A3
Comparison of SSA and SSI using 1st and 2nd order expansion

	Standard deviation	Order	−30 mV	−20 mV	−10 mV	0 mV	10 mV	20 mV	30 mV
SSA	5%	1st	0.033 ± 0.010	0.163 ± 0.032	0.408 ± 0.043	0.644 ± 0.033	0.804 ± 0.019	0.896 ± 0.010	0.948 ± 0.006
		2nd	0.033 ± 0.010	0.163 ± 0.032	0.408 ± 0.043	0.644 ± 0.033	0.804 ± 0.019	0.896 ± 0.010	0.948 ± 0.006
	10%	1st	0.036 ± 0.020	0.168 ± 0.065	0.408 ± 0.086	0.640 ± 0.065	0.800 ± 0.038	0.893 ± 0.020	0.945 ± 0.011
		2nd	0.036 ± 0.022	0.168 ± 0.064	0.408 ± 0.085	0.640 ± 0.065	0.799 ± 0.039	0.892 ± 0.021	0.945 ± 0.012
	Standard deviation	Order	−80 mV	−70 mV	−60 mV	−50 mV	−40 mV	−30 mV	−20 mV
SSI	5%	1st	0.994 ± 0.006	0.994 ± 0.006	0.993 ± 0.006	0.989 ± 0.006	0.934 ± 0.013	0.516 ± 0.052	0.075 ± 0.012
		2nd	0.994 ± 0.006	0.994 ± 0.006	0.993 ± 0.006	0.989 ± 0.006	0.934 ± 0.013	0.516 ± 0.052	0.075 ± 0.012
	10%	1st	0.988 ± 0.012	0.988 ± 0.012	0.988 ± 0.012	0.983 ± 0.012	0.926 ± 0.028	0.513 ± 0.099	0.077 ± 0.022
		2nd	0.988 ± 0.013	0.987 ± 0.012	0.987 ± 0.013	0.982 ± 0.013	0.925 ± 0.027	0.512 ± 0.100	0.078 ± 0.025

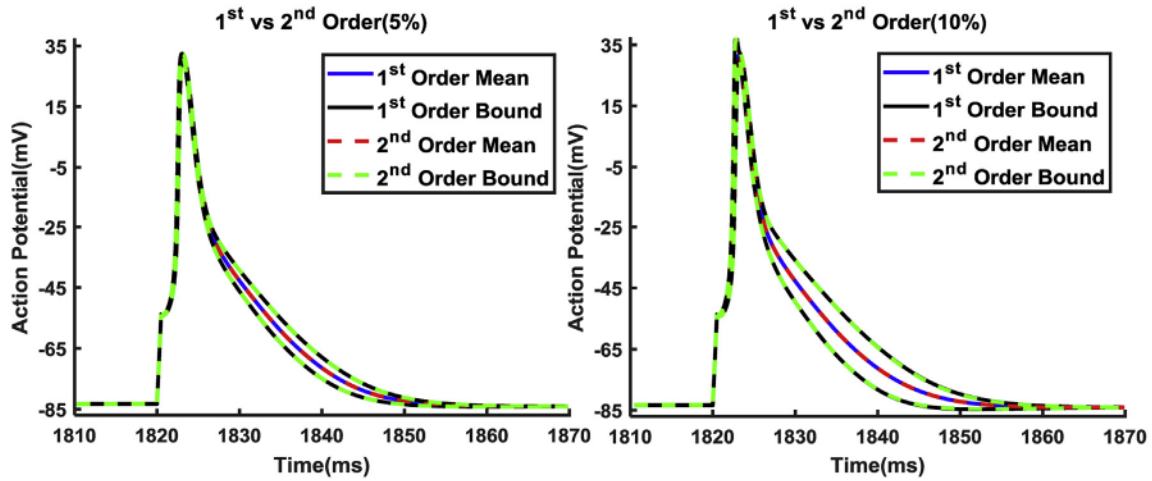

Fig. A3. Mean, upper, and lower bounds of AP obtained with gPC by using 1st and 2nd order expansion.3

References

[1] D. Noble, Cardiac action and pacemaker potentials based on the Hodgkin-Huxley equations, Nature 188 (4749) (1960) 495–497.
[2] D. Noble, A modification of the Hodgkin—Huxley equations applicable to Purkinje fibre action and pacemaker potentials, J. Physiol. 160 (2) (1962) 317.
[3] D. Du, et al., Statistical metamodeling and sequential design of computer experiments to model Glyco-altered gating of sodium channels in cardiac myocytes, IEEE J. Biomed. Health Inf. 20 (5) (2016) 1439–1452.
[4] H. Ashikaga, et al., Feasibility of image-based simulation to estimate ablation target in human ventricular arrhythmia, Heart Rhythm 10 (8) (2013) 1109–1116.
[5] N.A. Trayanova, P.M. Boyle, Advances in modeling ventricular arrhythmias: from mechanisms to the clinic, Wiley Interdiscipl. Rev. Syst. Biol. Med. 6 (2) (2014) 209–224.
[6] R. Chabiniok, et al., Multiphysics and multiscale modelling, data–model fusion and integration of organ physiology in the clinic: ventricular cardiac mechanics, Interface Focus 6 (2) (2016).
[7] P. Pathmanathan, et al., Uncertainty quantification of fast sodium current steady-state inactivation for multi-scale models of cardiac electrophysiology, Prog. Biophys. Mol. Biol. 117 (1) (2015) 4–18.
[8] R.H. Johnstone, et al., Uncertainty and variability in models of the cardiac action potential: can we build trustworthy models? J. Mol. Cell. Cardiol. 96 (2016) 49–62.
[9] A. Muszkiewicz, et al., Variability in cardiac electrophysiology: using experimentally-calibrated populations of models to move beyond the single virtual physiological human paradigm, Prog. Biophys. Mol. Biol. 120 (1) (2016) 115–127.
[10] M. Lemay, E. de Lange, J.P. Kucera, Effects of stochastic channel gating and distribution on the cardiac action potential, J. Theor. Biol. 281 (1) (2011) 84–96.
[11] J. Walmsley, et al., Application of stochastic phenomenological modelling to cell-to-cell and beat-to-beat electrophysiological variability in cardiac tissue, J. Theor. Biol. 365 (2015) 325–336.
[12] P. Pathmanathan, R.A. Gray, Verification of computational models of cardiac electro-physiology, Int. J. Numer. Meth. Biomed. Eng. 30 (5) (2014) 525–544.
[13] A.X. Sarkar, D.J. Christini, E.A. Sobie, Exploiting mathematical models to illuminate electrophysiological variability between individuals, J. Physiol. 590 (11) (2012) 2555–2567.
[14] D.E. Hurtado, S. Castro, P. Madrid, Uncertainty quantification of two models of cardiac electromechanics, Int. J. Numer. Meth. Biomed. Eng. 33 (12) (2017) e2894.
[15] L. Romero, et al., Impact of ionic current variability on human ventricular cellular electrophysiology, Am. J. Physiol. Heart Circ. Physiol. 297 (4) (2009) H1436–H1445.
[16] S.E. Geneser, et al., Stochastic Markovian modeling of electrophysiology of ion channels: reconstruction of standard deviations in macroscopic currents, J. Theor. Biol. 245 (4) (2007) 627–637.
[17] A. Quarteroni, A. Manzoni, C. Vergara, The cardiovascular system: mathematical modelling, numerical algorithms and clinical applications, Acta Numer. 26 (2017) 365–590.
[18] D. Xiu, Efficient collocational approach for parametric uncertainty analysis, Commun. Comput. Phys. 2 (2) (2007) 293–309.
[19] D. Xiu, G.E. Karniadakis, The Wiener–Askey polynomial chaos for stochastic differential equations, SIAM J. Sci. Comput. 24 (2) (2002) 619–644.
[20] D. Xiu, G.E. Karniadakis, Modeling uncertainty in steady state diffusion problems via generalized polynomial chaos, Comput. Meth. Appl. Mech. Eng. 191 (43) (2002) 4927–4948.
[21] K.-K.K. Kim, et al., Wiener's polynomial chaos for the analysis and control of nonlinear dynamical systems with probabilistic uncertainties [historical perspectives], IEEE Contr. Syst. Mag. 33 (5) (2013) 58–67.
[22] M. Asher, et al., A review of surrogate models and their application to groundwater modeling, Water Resour. Res. 51 (8) (2015) 5957–5973.
[23] G. Blatman, B. Sudret, Adaptive sparse polynomial chaos expansion based on least angle regression, J. Comput. Phys. 230 (6) (2011) 2345–2367.
[24] D. Xiu, S.J. Sherwin, Parametric uncertainty analysis of pulse wave propagation in a model of a human arterial network, J. Comput. Phys. 226 (2) (2007) 1385–1407.
[25] Y. Du, D. Du, Propagation of parametric uncertainty for the K+ channel model in mouse ventricular myocytes, Engineering in Medicine and Biology Society (EMBC), 2016 IEEE 38th Annual International Conference, 2016.
[26] V.E. Bondarenko, et al., Computer model of action potential of mouse ventricular myocytes, Am. J. Physiol. Heart Circ. Physiol. 287 (3) (2004) H1378–H1403.
[27] M. Eldred, J. Burkardt, Comparison of non-intrusive polynomial chaos and stochastic collocation methods for uncertainty quantification, 47th AIAA Aerospace Sciences Meeting Including the New Horizons Forum and Aerospace Exposition, 2009.
[28] Y. Du, H. Budman, T.A. Duever, Integration of fault diagnosis and control based on a trade-off between fault detectability and closed loop performance, J. Process Contr. 38 (2016) 42–53.
[29] J. Butcher, Runge-Kutta methods, Scholarpedia 2 (9) (2007) 3147.
[30] R. Clayton, et al., Models of cardiac tissue electrophysiology: progress, challenges and open questions, Prog. Biophys. Mol. Biol. 104 (1–3) (2011) 22–48.
[31] A. Workman, et al., Transient outward K+ current reduction prolongs action potentials and promotes after depolarisations: a dynamic-clamp study in human and rabbit cardiac atrial myocytes, J. Physiol. 590 (17) (2012) 4289–4305.
[32] Z. Zhao, et al., Role of the transient outward potassium current in the genesis of early afterdepolarizations in cardiac cells, Cardiovasc. Res. 95 (3) (2012) 308–316.
[33] A.R. Ednie, et al., Expression of the sialyltransferase, ST3Gal4, impacts cardiac voltage-gated sodium channel activity, refractory period and ventricular conduction, J. Mol. Cell. Cardiol. 59 (2013) 117–127.
[34] J.Y. Fang, et al., From competency to dormancy: a 3D model to study cancer cells and drug responsiveness, J. Transl. Med. 14 (1) (2016) 38.
[35] H. Nakamura, et al., Presence and functional role of the rapidly activating delayed rectifier K+ current in left and right atria of adult mice, Eur. J. Pharmacol. 649 (1–3) (2010) 14–22.
[36] N. Chiamvimonvat, et al., Potassium currents in the heart: functional roles in repolarization, arrhythmia and therapeutics, J. Physiol. 595 (7) (2017) 2229–2252.
[37] I.M. Sobol, Global sensitivity indices for nonlinear mathematical models and their Monte Carlo estimates, Math. Comput. Simulat. 55 (1–3) (2001) 271–280.
[38] J. Nossent, P. Elsen, W. Bauwens, Sobol'sensitivity analysis of a complex environmental model, Environ. Model. Software 26 (12) (2011) 1515–1525.
[39] A. Saltelli, Making best use of model evaluations to compute sensitivity indices, Comput. Phys. Commun. 145 (2) (2002) 280–297.
[40] R.A. Gray, A.M. Pertsov, J. Jalife, Spatial and temporal organization during cardiac fibrillation, Nature 392 (6671) (1998) 75.
[41] G.R. Mirams, et al., Uncertainty and variability in computational and mathematical models of cardiac physiology, J. Physiol. 594 (23) (2016) 6833–6847.
[42] S. Abraham, et al., A robust and efficient stepwise regression method for building sparse polynomial chaos expansions, J. Comput. Phys. 332 (2017) 461–474.
[43] A. O'Hagan, Polynomial chaos: a tutorial and critique from a statistician's perspective, SIAM/ASA J. Uncertain. Quantification 20 (2013) 1–20.
[44] Y. Du, H. Budman, T. Duever, Parameter estimation for an inverse nonlinear stochastic problem: reactivity ratio studies in copolymerization, Macromol. Theory Simul. 26 (2) (2017) 1–15.